https://doi.org/10.5194/egusphere-2026-4577
Preprint. Discussion started: 20 August 2026

Novel approaches for bridging chemical and biological time series observations to reveal underlying impacts of ocean acidification on marine organisms and ecosystems

Natalija Suhareva[1], Per J. Hansen[1], Yuri Artioli[2], Sam Dupont[3], Kirsten Isensee[4], Steve Widdicombe[5], Henrik O. Enevoldsen[6]

[1] Marine Biological Section, University of Copenhagen, Helsingør, 3000, Denmark
[2] Plymouth Marine Laboratory, Plymouth, PL13DH, United Kingdom
[3] Kristineberg Marine Research Station, University of Gothenburg, Fiskebäckskil, 45178, Sweden
[4] Intergovernmental Oceanographic Commission (IOC) of UNESCO, Paris, 75007, France
[5] Sharjah Marine Science Research Centre, University of Khrofakkan, Khrofakkan, 18119 United Arab Emirates
[6] Intergovernmental Oceanographic Commission (IOC) of UNESCO, Helsingør, 3000, Denmark

Correspondence to: Natalija Suhareva (natalija.suhareva@bio.ku.dk)

Abstract. There is increasing demand to compare long-term biological observations with derived or measured carbonate chemistry data to characterize the biological consequences of ocean acidification (OA) in natural environments. Meeting this need calls for a standardized methodology by which to quantify and directly compare biological and carbonate chemistry change. Widdicombe et al. (2023) proposed a conceptual framework based on biological traits and paired biological-chemical rate comparisons, but its practical implementation has remained unresolved.

Here we operationalize that conceptual framework through a standardized analytical workflow that integrates heterogeneous biological observations with established OA time series methodology. The workflow addresses five analytical challenges that hinder comparison of long-term biological and OA records: 1) fundamentally different temporal structures of biological and OA time series, 2) heterogeneity of biological observations, 3) sparse and irregular biological sampling, 4) nonlinear biological trajectories, and 5) appearance–disappearance events that invalidate conventional relative change metrics. The workflow addresses these challenges through standardized biological grouping, annual aggregation, piecewise linear segmentation, normalization by ecological boundaries, and direct pairing of biological and chemical rates of change.

We evaluated workflow performance using 36 synthetic biological time series generated by applying predefined temperature-pH-driven biological performance functions to a 108-year hydrodynamic-biogeochemical model simulation under the SSP3-7.0 emissions scenario. Biological rates estimated by the workflow closely agreed with the corresponding reference rates. Rate estimates remained similar across the two annual representations, and their relative ordering was largely preserved across contrasting site-specific temperature-pH transitions. These results demonstrate the robustness of the workflow under the tested patterns of abiotic forcing.

The analytical workflow developed here operationalizes the conceptual approach of Widdicombe et al. (2023) by standardizing the estimation and comparison of rates of change in biological and carbonate chemistry time series. It supports

https://doi.org/10.5194/egusphere-2026-4577
Preprint. Discussion started: 20 August 2026

comparisons among compatible biological indicators while retaining the ecological context of each time series. The workflow does not establish causality; instead, it assesses the temporal coherence between long-term changes in candidate biological indicators of OA and concurrent changes in carbonate chemistry. It therefore provides a practical foundation for regional and global syntheses of biological responses to OA and other long-term abiotic stressors.

1 Introduction

The ocean is undergoing sustained physical, chemical, and ecological transformations driven by human-induced increases in atmospheric carbon dioxide (CO_2) concentrations. Among these transformations is a phenomenon called ocean acidification (OA), caused primarily by the uptake of atmospheric CO_2 by the surface ocean (Friedlingstein et al., 2026; Gruber et al., 2019). This uptake alters seawater carbonate chemistry, lowers pH, and affects physiological and ecological processes (Gattuso and Hansson, 2011). These changes occur alongside other climate related stressors, including warming, deoxygenation, extreme events, and altered circulation, producing complex and spatially variable abiotic conditions (Gruber et al., 2021). In addition to atmospheric forcing, regional processes such as local biology and physiology, upwelling, freshwater inputs, and sea-ice dynamics modify the carbonate system (Qi et al., 2024; Schmidt et al., 2025; Wright-Fairbanks and Saba, 2022). Consequently, species and ecosystems are exposed to different levels of variability in carbonate chemistry depending on their habitat, behaviour, and geographical distribution, shaping their sensitivity to OA through local adaptation (Vargas et al., 2017, 2022).

Despite decades of research (Ma et al., 2023; Yang et al., 2024, 2016), and the wealth of evidence that has been amassed from controlled laboratory and field experiments, the ability to detect and compare biological responses to OA across natural systems remains markedly limited (from OA-ICC biological response data compilation, last checked in July 2026; Yang et al., 2024). Although there are recognized regional restrains in capacity and data availability (Tilbrook et al., 2019), this limitation arises less from a lack of observations than from the absence of a consistent analytical framework for integrating biological time series and chemical observations of OA (Widdicombe et al., 2023). Previous approaches addressed the challenge of comparing responses across studies and systems by analysing the relative change from a defined baseline (Bednaršek et al., 2019; Busch and McElhany, 2016; Kroeker et al., 2013; Wittmann and Pörtner, 2013). Although useful for comparing effect magnitudes, baseline-relative change does not quantify concurrent rates of biological and carbonate chemistry change or their temporal relationship.

Widdicombe et al. (2023) proposed a new conceptual framework, based on comparing rates of biological and carbonate chemistry change. The framework aims to detail the generality of biological impacts of OA by embracing the variety of different biological observations and data that could be available (Muller-Karger et al., 2018). However, practical application of this idea has remained limited by the absence of a standardized workflow for aligning, and joint analysis of biological and carbonate chemistry time series.

https://doi.org/10.5194/egusphere-2026-4577
Preprint. Discussion started: 20 August 2026

Recent efforts have substantially improved the standardization and precision of carbonate chemistry measurements and OA trend detection (Dickson et al., 2007; Riebesell and Gattuso, 2015; UNESCO/IOC, 2019). Sutton et al. (2022) established robust best practices for estimating long-term change from OA time series. In contrast, biological time series rarely follow standardized formats (Bayraktarov et al., 2019; Benson et al., 2022; Bowler et al., 2025), leading to widespread gaps in taxonomy, space, and time (Muller-Karger et al., 2018). The International Group for Marine Ecological Time Series (IGMETS) report (O'Brien et al., 2017) identified major gaps in biological monitoring consistency and emphasized the need for sustained quality-controlled observations. They revealed that long-term monitoring datasets may differ in sampling gear, counting method, analytical protocol, sampling depth, taxonomic resolution, and measurement units. IGMETS explicitly noted that such values are "not easily intercomparable, if at all", but that time series analysis can still compare how variables change relative to themselves and to each other, provided that the method used within each time series remains internally consistent. The international community has focused considerable progress in standardizing biological observations. Harmonized observing frameworks, Essential Ocean Variables (EOVs), interoperable biodiversity databases, FAIR data practices, and community-endorsed best practices have improved the comparability, accessibility, and reuse of marine biodiversity observations (Canonico et al., 2019; Ingenloff et al., 2025; Klein et al., 2019; Lawrence et al., 2026; Muller-Karger et al., 2018; Pearlman et al., 2021; Saeedi, 2026). However, mobilizing the scientific community to align sampling strategies with the principles defined in the EOV specification sheets remains a major challenge (Klein et al., 2019; Muller-Karger et al., 2018; Saeedi, 2026), because temporal resolution and spatial extent of data collections remains limited (Kaplanis, 2023).

Both biological and physicochemical observations provide complementary information about marine ecosystem state and are increasingly integrated within sustained ocean observing systems (Miloslavich et al., 2018; Smit et al., 2021). Carbonate chemistry time series are typically represented as continuous long-term trends after removing periodic variability (Bates et al., 2014; Bates, 2001; Sutton et al., 2022; Takahashi et al., 2009). Biological response trajectories, however, may include thresholds, delayed responses, phase shifts, and abrupt community reorganizations (Andersen et al., 2009; Bode, 2024; Conversi et al., 2015; deYoung et al., 2008). These contrasting temporal structures require distinct analytical treatment: physicochemical change is estimated over the full analysis window, whereas biological change may be estimated separately within temporal segments whose breakpoints are defined from the biological time series. Applying identical analytical assumptions to both domains could obscure biologically meaningful dynamics.

Here we propose a standardized analytical workflow that operationalizes the conceptual framework developed by Widdicombe et al. (2023). Building on their trait-based approach, which organizes biological observations into five broad trait families applicable across most marine ecosystems, the workflow transforms heterogeneous biological observations into standardized biological rates of change that can be directly compared with rates derived from carbonate chemistry observations. It is designed to address five recurring analytical challenges: (1) the distinct analytical requirements of biological and physicochemical time series; (2) the inherent heterogeneity of biological variables, which limits direct comparison; (3) the unequal ability to resolve temporal dynamics resulting from sparse and irregular biological sampling; (4)

https://doi.org/10.5194/egusphere-2026-4577
Preprint. Discussion started: 20 August 2026

the potential for single linear trends to misrepresent nonlinear biological trajectories; and (5) undefined relative rates when trajectories begin or end at zero, as occurs during appearance and disappearance events.

The objectives of this work are therefore twofold: (1) to formalize a methodological framework for integrating long-term biological and carbonate chemistry or, more broadly, biological and physicochemical time series (hereafter referred to as biotic and abiotic time series, respectively); and (2) to evaluate the performance of the proposed workflow using a controlled test case generated from model-derived data.

To demonstrate and evaluate the workflow, we used 108 years of temperature and pH data generated by a coupled hydrodynamic-biogeochemical model. We paired six temperature performance functions with six pH performance functions to generate 36 noise-free biological response trajectories. We then added observational noise to create the corresponding synthetic biotic time series and applied the workflow to the paired biotic and abiotic data. Finally, we assessed its transferability across four contrasting site-specific temperature-pH transitions over the 108-year period, represented by two surface and two bottom-water time series.

By translating a conceptual framework into an explicit analytical structure, this work provides a foundation for consistent, cross-site evaluation of biological responses to OA and supports the integration of biological indicators into long-term observing systems. As such, this methodology seeks to accelerate progress towards a comprehensive assessment of real-world biological impacts that are wholly or partially driven by OA.

2. Analytical workflow

2.1 Conceptual analytical workflow

The workflow consists of two principal analytical streams, biotic and abiotic, to accommodate these distinct analytical requirements between biotic and abiotic time series. In the abiotic stream, physicochemical change is represented by a continuous, long-term rate estimated after removing seasonal variability, capturing sustained forcing over the full observation period. In the biotic stream, biological change is represented as a sequence of, at maximum, two internally consistent linear segments, capturing non-linear and phase-dependent responses. In the end the estimated rates of change are paired together (Fig. 1).

2.2 Scope of the abiotic component

Preprocessing of the abiotic component of the framework follows established best-practice recommendations for the assessment of OA time series trends (Sutton et al., 2022). We therefore do not redefine OA trend methodology here.

In general, abiotic observations should be collected at a sufficiently high temporal resolution to resolve seasonal and other dominant modes of natural variability before estimating long-term trends (Carter et al., 2019; Sutton et al., 2022, 2019; Turk et al., 2019). In highly dynamic coastal environments, more frequent observations may be required to characterize extreme

https://doi.org/10.5194/egusphere-2026-4577
Preprint. Discussion started: 20 August 2026

events and episodic variability associated with processes such as upwelling, river discharge, and biological metabolism
130 (Vargas et al., 2022, 2017).

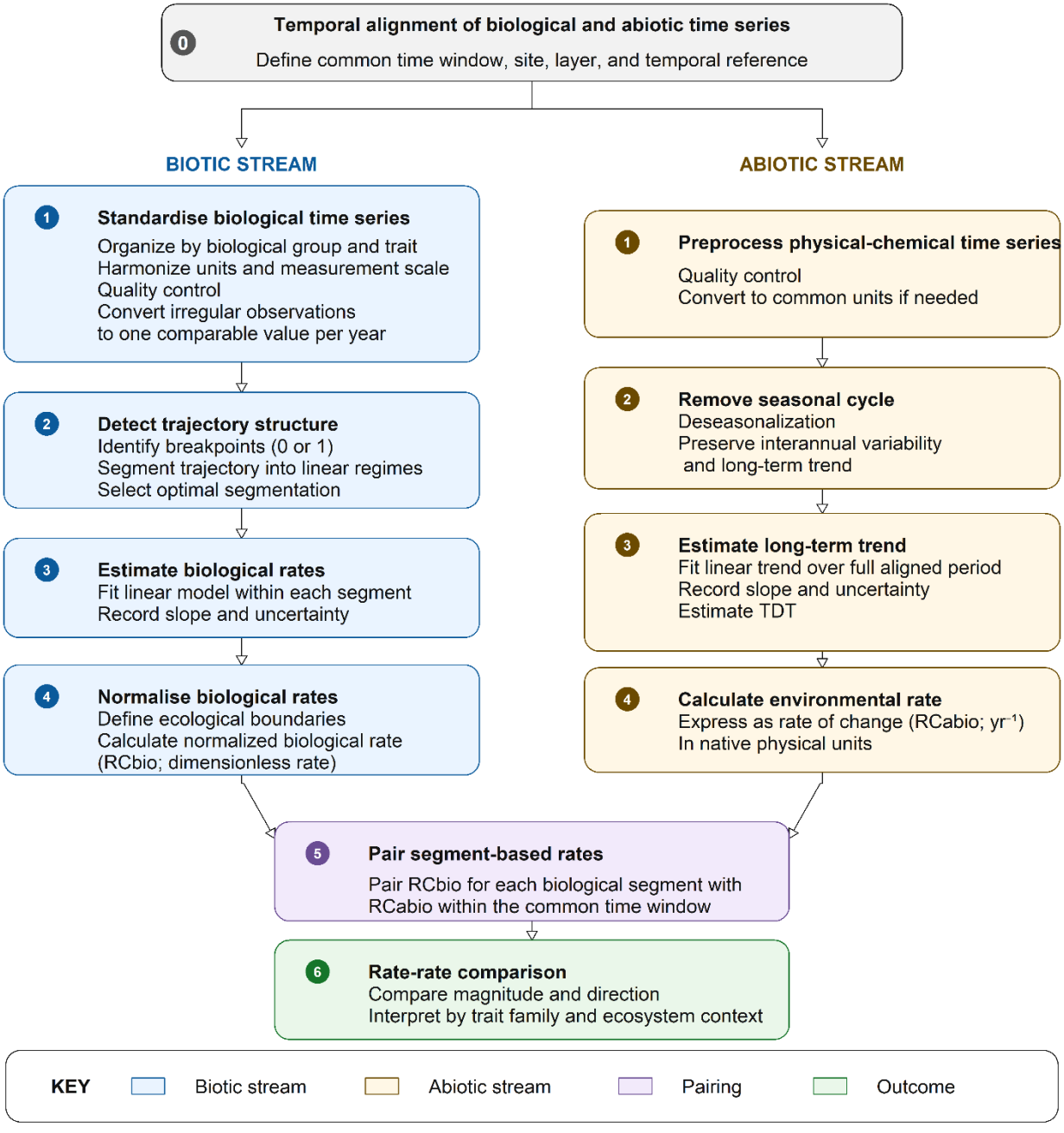

Figure 1. Conceptual workflow for estimating and pairing biological and physicochemical rates of change. Biotic stream analyses biological time series; abiotic stream analyses carbonate chemistry and other physicochemical time series. RCbio – rate of change of a biotic variable; RCabio – rate of change of an abiotic variable; TDT – the trend detection time.

https://doi.org/10.5194/egusphere-2026-4577
Preprint. Discussion started: 20 August 2026

Following the best-practice recommendations of Sutton et al. (2022), the workflow proposed here removes the mean seasonal cycle using their deseasonalisation procedure before estimating long-term change. This procedure preserves interannual variability while removing recurring seasonal patterns. For each deseasoned abiotic time series, the workflow uses the Trend Detection Time (TDT) approach to estimate the time required to detect a statistically significant trend (Sutton et al., 2022; Weatherhead et al., 1998). It then calculates the rate of physicochemical change as the slope of a single ordinary least-squares linear regression fitted to the full deseasoned time series.

2.3 Scope of the biotic component

2.3.1 Problem overview

Biotic observations may represent entity-level measured variables, such as taxonomic abundance, biomass, cover, or ecosystem process variables as productivity, phenological metrics, and community metrices, e.g., biodiversity indices and trophic richness. Each different set of biological observations can differ in their units, sampling designs, objectives, analytical protocols, ecological scope, and expected response dynamics. Therefore, several issues need to be addressed prior to the biological rate-of-change estimation. The issues can be largely classified into four main groups, covering: 1) impossible direct comparability of traits, 2) unequal ability to resolve temporal dynamics, 3) inadequacy of linear trend resolving complex dynamics, and 4) phenomena of appearance and disappearance of biological entities (Table 1).

Table 1. Analytical challenges addressed by the proposed biological rate-of-change framework and the corresponding workflow solutions.

Problem	Cause	Framework response
Biological variables are not directly comparable	Heterogenous time series designs	Standardization into biological groups and traits
Unequal ability to resolve temporal dynamics	Irregular and infrequent sampling	Aggregation to a common annual representation
Single linear trends may misrepresent long-term change	Non-linear ecological trajectories	Segmentation into locally linear intervals
Relative rates become undefined when trajectories start or end at zero	Appearance and disappearance of biological entities	Transformation to bounded relative metrics

2.3.2 Standardization into biological groups and traits

To operationalize the above concepts, we recommend first converting biological data into a tidy (long) format (Wickham, 2016, 2014), and standardizing observations into analytical time series units before estimating rates of change. Each analytical unit is defined by two components:

https://doi.org/10.5194/egusphere-2026-4577
Preprint. Discussion started: 20 August 2026

(1) *Biological group*: the biological subject of assessment, whose response is evaluated through time. A biological group may have one or multiple categories. Depending on the dataset, a biological group may correspond to an entity-level biological variable, a community-level metric, or an ecosystem process variable, e.g., taxonomic group, functional group, size class, community-level metric, ecosystem process, or other biological variable, depending on the structure of the dataset.

(2) *Biological trait value*: the observation, measurement, or derived metric used to characterize a biological group (e.g., abundance, biomass, calcification rate, pigment concentration, diversity index value).

Each category of a biological group forms a unique trajectory of its biological trait value through the analysed time window, representing a single biological response to physicochemical change – the *time series unit*. The workflow estimates rates of change independently for each time series unit.

2.3.3 Aggregation to a common annual representation

The type of biological information that can be extracted from time series depends primarily on sampling frequency and biological group resolution. Finely resolved datasets support entity-specific interpretation, whereas more broadly aggregated biological groups may capture community or ecosystem dynamics. High-frequency datasets can support analysis of within-year dynamics, such as bloom timing, bloom duration, seasonal succession, or phenological shifts. In contrast, low-frequency datasets may not support reliable reconstruction of temporal dynamics and are better suited to aggregated state metrics, such as annual mean abundance, seasonal mean biomass, annual productivity, or time-integrated community indicators. Figure 2 conceptualizes the relationship between dataset structure and the level of ecological interpretation that can be supported.

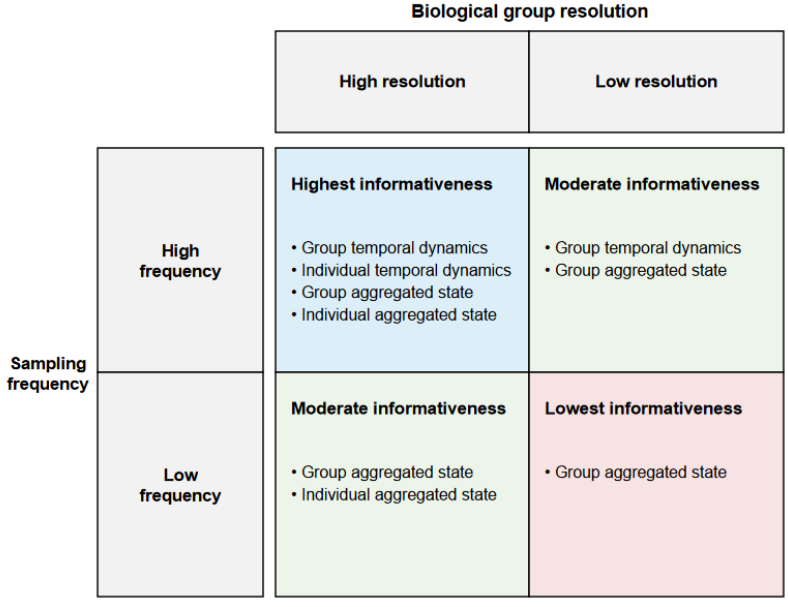

Figure 2. Conceptual relationship between sampling frequency, biological group resolution, and the level of ecological information that can be extracted from biotic time series.

https://doi.org/10.5194/egusphere-2026-4577
Preprint. Discussion started: 20 August 2026

Within this framework we suggest generating one annual biological trait value per biological group. For example, depending on the ecological context and data informativeness of the data, researchers may use a single observation, the mean for a selected month, or a seasonal mean as the representative annual value.

2.3.4 Segmentation into locally linear intervals

To balance comparability and ecological realism, we suggest representing biological response trajectories as one or two internally consistent linear segments. Most time series are expected to remain adequately represented by a single trend. The two-segment limit is pragmatic: short, irregular, and highly variable biological records rarely support reliable estimation of multiple breakpoints, which may instead fit sampling noise or interannual variability. The pairwise linear segmentation approach follows the logic of segmented straight-line approximation and partition regression, in which an ordered trajectory is divided into contiguous intervals and separate linear models are fitted within each interval (Bellman and Roth, 1969; Guthery, 1974; Muggeo, 2003). For each biotic time series, the workflow evaluates two alternative representations: (i) a single full-period linear trend and (ii) a two-segment linear trajectory separated by one breakpoint.

For a biological response trajectory defined as:

$$\{(x_i, y_i)\}_{i=1}^{n}, \quad (1)$$

where x_i is calendar year, expressed as a numeric variable, and y_i is the standardized biological trait value. Then the single-segment model is:

$$y_i = \beta_0 + \beta_1 x_i + \varepsilon_i, \quad (2)$$

where β_0 is the intercept, β_1 is the full-period slope of biological response, and ε_i is the residual error.

For a candidate breakpoint τ, the time series are divided into two contiguous intervals:

$$S_1 = \{x_i : x_i \leq \tau\}, \quad (3)$$

$$S_2 = \{x_i : x_i > \tau\}. \quad (4)$$

The workflow then fits separate linear models within each segment:

$$y_i = \begin{cases} \alpha_1 + \beta_1 x_i + \varepsilon_i, & x_i \leq \tau, \\ \alpha_2 + \beta_2 x_i + \varepsilon_i, & x_i > \tau, \end{cases} \quad (5)$$

where α_1 and α_2 are segment-specific intercepts, and β_1 and β_2 are segment-specific change slopes. For each candidate breakpoint, the total residual sum of squares is calculated as:

$$SSE_2(\tau) = \sum_{x_i \leq \tau} (y_i - \hat{y}_{1,i})^2 + \sum_{x_i > \tau} (y_i - \hat{y}_{2,i})^2, \quad (6)$$

where $\hat{y}_{1,i}$ and $\hat{y}_{2,i}$ are fitted values from the first and second segment models, respectively.

The workflow defines the optimal breakpoint as the value minimizing the total within-segment residual error (Bellman and Roth, 1969; Guthery, 1974):

$$\tau^* = \arg\min_{\tau} SSE_2(\tau). \quad (7)$$

Selection between the single-segment and two-segment representations is based on the Bayesian Information Criterion (BIC), following the general principle of complexity-penalized change-point selection (Yao, 1988):

https://doi.org/10.5194/egusphere-2026-4577
Preprint. Discussion started: 20 August 2026

$$BIC = n \ln\left(\frac{SSE}{n}\right) + k \ln(n), \quad (8)$$

where n is the number of observations, *SSE* is the residual sum of squares, and *k* is the number of estimated parameters. The single-segment model uses (*k=2*), corresponding to the intercept and slope. The two-segment model uses (*k=5*), corresponding to two intercepts, two slopes, and the estimated breakpoint. The workflow accepts segmentation only when:

$$BIC_{two} < BIC_{single}. \quad (9)$$

If the two-segment model does not improve the BIC, or if either segment failed to satisfy the minimum data requirements for slope estimation, the workflow retains the full-period linear model. The resulting slope or slopes are used as biological rates of change for comparison with physicochemical rates over the corresponding time intervals.

2.3.5 Transformation to bounded relative metrics for rate-of-change estimation

The next step of the workflow is to quantify the rates of change using domain-specific procedures. In the biotic stream, the rates are calculated separately for each defined segment, while in the abiotic stream, a single rate is calculated once over the full aligned analysis window.

For each biological respose segment s_i, spanning the interval $[x_{1,s_i}, x_{2,s_i}]$, the workflow estimates predicted biological trait values from the segment-specific linear model:

$$\hat{Y}^{bio}_{start,s_i} = a_{s_i} + b_{s_i} x_{1,s_i}, \hat{Y}^{bio}_{end,s_i} = a_{s_i} + b_{s_i} x_{2,s_i}, \quad (10)$$

where a_{s_i} and b_{s_i} denote the intercept and slope of the segment model. The absolute biological rate of change is calculated as:

$$RC^{bio}_{s_i} = \frac{\hat{Y}^{bio}_{end,s_i} - \hat{Y}^{bio}_{start,s_i}}{x_{2,s_i} - x_{1,s_i}}. \quad (11)$$

Comparisons of biological change are restricted to biological response representing the same level of biological organization. To account for differences in units and magnitude, the workflow applies min–max normalization with the lower biological boundary fixed at zero (Asesh, 2022). For each fitted segment, the larger of the predicted values at its beginning and end defines the upper boundary. The normalized biological values therefore range from 0 to 1, while the corresponding biotic rate expresses annual change relative to the segment maximum:

$$RC^{bio}_{s_i}(\%) = 100 \times \frac{RC^{bio}_{s_i}}{max(\hat{Y}^{bio}_{start,s_i}, \hat{Y}^{bio}_{end,s_i})}. \quad (12)$$

In the abiotic stream, a single linear model is fitted to the deseasoned time series over the full aligned analysis window $S_0 = [x_{1,S_0}, x_{2,S_0}]$. From this model, predicted physicochemical values are calculated as:

$$\hat{Y}^{abio}_{start,S_0} = \alpha + \omega x_{1,S_0}, \hat{Y}^{abio}_{end,S_0} = \alpha + \omega x_{2,S_0}, \quad (13)$$

where ω is the full-period slope. In turn, the rate of change is calculated as:

$$RC^{abio}_{S_0} = \frac{\hat{Y}^{abio}_{end,S_0} - \hat{Y}^{abio}_{start,S_0}}{x_{2,S_0} - x_{1,S_0}}. \quad (14)$$

The workflow retains abiotic rates in their native physical units per year.

The next step is to pair each biotic rate per segment with the same full-window abiotic rate:

https://doi.org/10.5194/egusphere-2026-4577
Preprint. Discussion started: 20 August 2026

$$\left(RC_{s_i}^{bio}(\%), RC_{S_0}^{abio}\right). \quad (15)$$

Thus, a biotic time series represented by one segment yields one paired estimate. A time series represented by two segments yields two paired estimates, each containing a segment-specific biotic rate and the same full-window abiotic rate:

$$\left(RC_{s_1}^{bio}(\%), RC_{S_0}^{abio}\right), \left(RC_{s_2}^{bio}(\%), RC_{S_0}^{abio}\right). \quad (16)$$

3. Controlled test dataset for method demonstration

3.1 Modelled temperature and pH time series and transition-window definition

To evaluate the proposed framework under controlled conditions, we generated synthetic biotic time series with predefined temporal response trajectories within a defined abiotic transition window. We used temperature and pH as the abiotic drivers.

The temperature and pH time series were derived from the coupled hydrodynamic-biogeochemical model NEMO-ERSEM (Butenschön et al., 2016; Gurvan et al., 2019) simulating the dynamic of the North Western European Shelf at 7 km horizontal resolution. The simulation used here covers the period 1993-2100 and it was forced using atmospheric forcing and lateral boundary condition from the Earth System Model CNRM-ESM2-1 (Séférian et al., 2019) under the emission scenario SSP3-7.0 (corresponding to a realistic high emission scenario).

Method development was based on a single bottom-water time series from the Skagerrak (11.11°E, 58.53°N; hereafter **Site 1**), which was used for generation of biological response trajectories, and framework evaluation. To assess robustness under contrasting abiotic conditions, an additional three modelled time series were included: surface waters from the same location in the Skagerrak (**Site 2**), bottom waters from the North Sea (2.33°E, 57.40°N, hereafter **Site 3**), and surface waters from the same North Sea location (**Site 4**). Due to the vertical discretisation of the water column in the model, surface waters values come from 0.5 m below the surface and bottom water data from 2 m above the seafloor (that is located between 230 m and 240 m below the surface in all sites). These datasets introduced differences in seasonal variability and long-term OA trajectories, without considering local adaptation.

For each site and abiotic driver, we defined the transition window using mean June conditions calculated for the first and last ten years of the simulation. Hydrogen ion concentration ($[H^+]$) was additionally used for cross-station comparisons.

3.2 Generation of biological response trajectories

Generation of the simulated biological trajectories involved three distinct steps: definition of the driver-specific performance functions, computation of driver-combined biological response trajectories, and generation of nose-added synthetic biological time series from daily temperature and pH values.

For each abiotic driver, we defined a simplified trapezoidal performance function defined by four thresholds: $X_{low,0}$ is the value of the abiotic driver below which the performance curve is equal to 0, $X_{opt,min}$, $X_{opt,max}$ are the lower and upper bound of

https://doi.org/10.5194/egusphere-2026-4577
Preprint. Discussion started: 20 August 2026

the optimal window where the performance curve is equal to 1, $X_{high,0}$ is the value above which the performance curve is equal to 0 again (Table A1, and Fig. A1a and b). The full June range determined the lower and upper zero-performance limits, whereas the transition window between the first- and last-decade mean June conditions determined the optimal plateau boundaries.

For both temperature and pH, we defined six driver-specific performance functions (Fig.S1a and b): (T1 and P1) neutral, with optimal performance across the full abiotic transition window; (T2 and P2) hump-shaped, with a narrow optimum centred on the abiotic transition midpoint; (T3 and P3) positive, with the optimum located right after the end of the abiotic transition window; (T4 and P4) negative, representing the inverse pattern; (T5 and P5) threshold-positive, producing a rapid increase around the transition midpoint; and (T6 and P6) threshold-negative, producing the corresponding rapid decline. Pairing the six temperature-performance functions with the six pH-performance functions yielded 36 joint temperature-pH biological response trajectories.

We assumed that temperature and pH affected normalized biological performance independently and multiplicatively. Consequently, each driver scales the performance remaining under the other:

$$F_{combined} = F_T \times F_P, \quad (17)$$

where F_T and F_P are independently evaluated normalized performance values of temperature-performance and pH-performance functions, respectively. Each value represents the proportion of potential biological performance retained under the corresponding driver. Combined performance therefore reaches 1 only when both drivers permit maximum performance, whereas a value of 0 for either driver produces zero combined performance. This separable co-limitation formulation does not allow temperature to modify the pH-response function, or vice versa. It was used as a bounded null model for generating controlled synthetic trajectories rather than as an organism-specific model of multiple-driver effects.

Each pair of combined performance functions produced a two-dimensional temperature-pH performance surface in which each point represents the relative suitability under specific abiotic conditions (Fig. A1c). The modelled abiotic transition window then defined a directional path through the performance surface, connecting the mean conditions at the beginning and end of the simulation period (the black arrows in Fig. A1c).

Each of the 36 temperature-pH performance surfaces defined relative biological performance as a function of temperature and pH. To generate the noise-added synthetic biological time series, we evaluated each performance surface function using the daily temperature and pH values from the modelled abiotic time series throughout the 108-year simulation:

$$P_{j,t} = F_j(T_t, pH_t), j = 1, \dots, 36. \quad (18)$$

The resulting daily biological performance values retained the seasonal and short-term variability present in the abiotic inputs. For workflow demonstration and evaluation, we used mean June performance as the annual biological representation (Fig. A2). To assess the influence of annual sampling representation on long-term rate estimates, we compared rates derived from mean June performance with those derived from performance on 1 June. For the subsequent cross-site comparison, we generated noise-free biological time series by evaluating the same surface functions along the corresponding deseasoned temperature and pH trends of all four sites.

https://doi.org/10.5194/egusphere-2026-4577
Preprint. Discussion started: 20 August 2026

3.3 Framework performance evaluation design

Because the biological response trajectories were known, they provided reference quantities against which the workflow estimates could be evaluated. We compared the workflow-estimated rates with the corresponding reference rates, and the estimated breakpoint years versus the predefined ones.

We quantified the agreement between the reference and the estimated rates evaluating its regression slope, intercept, coefficient of determination (R^2), and root mean square error (RMSE). Because the method also estimates breakpoint timing, we additionally calculated the median absolute breakpoint error to evaluate accuracy of breakpoint estimation. The breakpoint error was calculated as the absolute difference between the reference and estimated breakpoint year.

We evaluated the annual aggregation step by comparing rates reconstructed from mean June performance with those reconstructed from performance on 1 June. Applying the Bland-Altman analysis (mean difference ± 1.96 SD, where SD is the standard deviation of the paired differences), we quantified systematic agreement between the two annual representations, while RMSE summarized the average magnitude of disagreement.

Finally, we assessed whether the relative ordering of biological rates remained consistent across sites with contrasting long-term temperature and pH transitions. We retained the same driver-specific performance-function shapes at all sites but recalculated their numerical parameters from each site-specific temperature and pH time series. We estimated and ranked the biological rates within each site and calculated pairwise Spearman rank correlations between sites. These correlations quantified the extent to which the relative ordering of biotic rates was preserved across contrasting site-specific transitions.

All workflow implementation, response scenario generation, statistical analyses, and visualization were performed in R version 4.5.1 (R Core Team, 2025). Biotic and abiotic rates of change were calculated using RoC workflow tool, developed within this study and is now available from the project's GitHub repository (https://github.com/OAPoCfNRS/RoC-tool).

4. Method demonstration

4.1 Deseasoned abiotic trends

Deseasonalisation removed the seasonal signal while preserving the long-term trajectories used for rate estimation (Fig. 3). Hydrogen ion concentration ($[H^+]$) followed the expected nonlinear increase because of the logarithmic relationship between pH and proton concentration. Consequently $[H^+]$ exhibited longer TDT (19 years) than it was for pH. The pH time series showed a monotonic decline with a short trend detection time (TDT = 12.3 years), whereas temperature exhibited substantially higher seasonal variability and a longer TDT (46.6 years), indicating slower emergence of the long-term signal despite a clear warming trend. Corresponding deseasoned trends for Sites 2-4 are shown in Fig. A3-5.

https://doi.org/10.5194/egusphere-2026-4577
Preprint. Discussion started: 20 August 2026

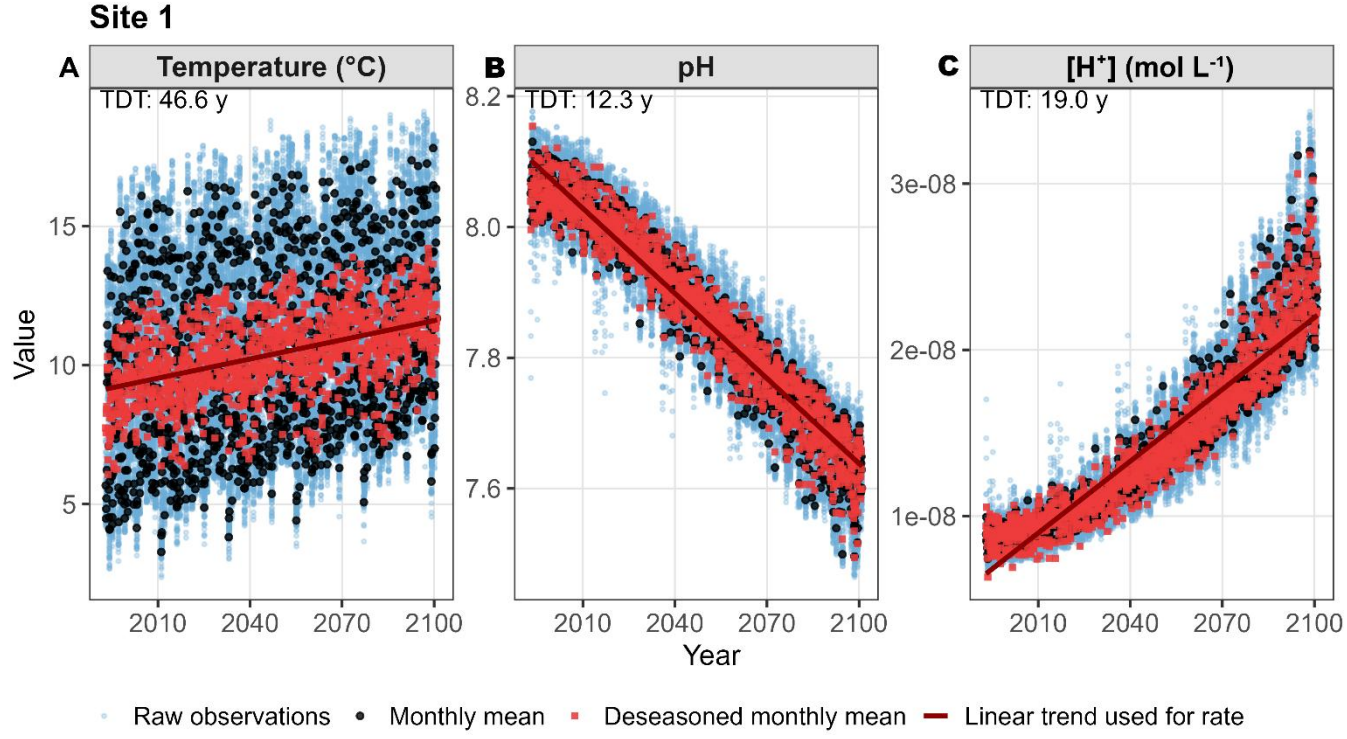

Figure 3. Deseasoned long-term trajectories of (A) temperature (°C), (B) hydrogen ion concentration ([H^+], mol L^{-1}), and (C) pH at Site 1 for 1993-2100. Light-blue points show the original model output, black points show monthly means, and red points show the corresponding deseasoned monthly mean values. Solid dark red lines represent the estimated long-term trends. The trend detection time (TDT) is represented in years.

4.2. Linear segmentation results

4.2.1. Estimation of biological response trajectory

Figure 4 illustrates how the temperature-pH performance surfaces presented in Fig. A1c were translated into temporal biological response trajectories and subsequently analysed by the workflow. The six examples combine the neutral temperature-response function (T1) with each of the six pH-response functions (P1-P6) and therefore correspond to the six performance surfaces in the top row of Fig. A1c. For each trajectory, the left panel shows the reference performance trajectory along the Site 1 abiotic transition window, the middle panel shows its noise-free segmented fit, and the right panel shows the noise-added simulated biotic time series and their segmented fit.

The fitted models generally preserved the main direction and phase structure of the simulated trajectories. Monotonic trajectories (T1-P3 and T1-P4) retained their expected direction and approximate slope, whereas the hump-shaped trajectory (T1-P2) was represented by two response phases separated by a breakpoint near the central optimum. For the threshold-like trajectories (T1-P5 and T1-P6), the principal pre- and post-breakpoint phases were generally identified, although the estimated secondary-segment slopes sometimes deviated from their reference values.

https://doi.org/10.5194/egusphere-2026-4577
Preprint. Discussion started: 20 August 2026

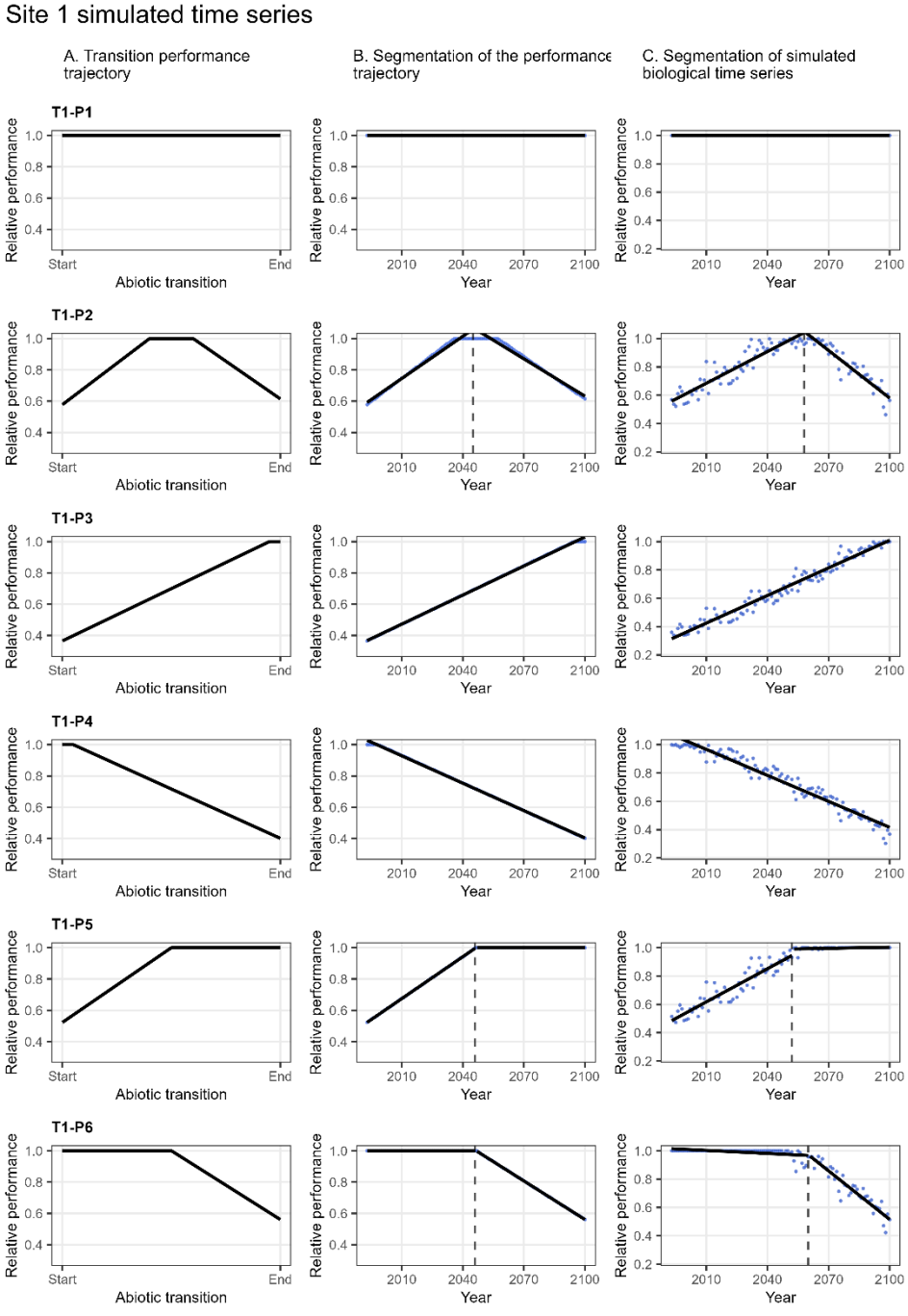

Figure 4. Translation of temperature-pH performance surfaces into simulated biological trajectories and segmented fits at Site 1. The six rows combine the neutral temperature-response function (T1) with the six pH-response functions (P1-P6) and correspond to the six surfaces in the top row of Figure A1. (A) The left column shows the reference performance profile along the Site 1 start-to-end temperature-pH transition path shown in Figure A1. (B) The middle column shows the resulting noise-free temporal

https://doi.org/10.5194/egusphere-2026-4577
Preprint. Discussion started: 20 August 2026

355 **trajectory (blue) and its fitted linear or one-breakpoint model (black). (C) The right column shows the corresponding noise-added simulated biological time series (blue) and fitted model (black). Vertical dashed lines indicate estimated breakpoints.**

The same comparison for the remaining biological response trajectories is presented in appendix Figures A6-10. Monotonic responses (e.g., T1-P3, T3-P3, T1-P4 and T3-P4) reproduced the expected response direction and overall slope, while hump-shaped responses (e.g., T1-P2, T3-P2 and T5-P2) preserved both response phases, placing the breakpoint at the transition
360 between them at the plateau area. Threshold responses in most cases reconstructed the dominant trajectory regimes, however a certain discrepancy occurred after breakpoint transitions (e.g., T1-P5, T1-P6, T5-P5 and T5-P6), the secondary segment frequently deviated from the expected slope, particularly in T5-P5 and T5-P6.

4.2.2. Segmentation validation

The framework estimated biotic rates that closely agreed with the corresponding reference rates across the simulated
365 response scenarios. (Fig. 5a). Estimated and reference rates showed strong agreement (R^2 = 0.969, RMSE = 0.002, Table A2), with a regression slope of 0.92 and an intercept close to zero (-0.0007), indicating only minor systematic underestimation of the highest rates. Agreement was maintained across all response trajectories. The largest deviations from the 1:1 relationship occurred only for trajectories with the strongest positive and negative rates, whereas intermediate responses were reconstructed almost exactly.

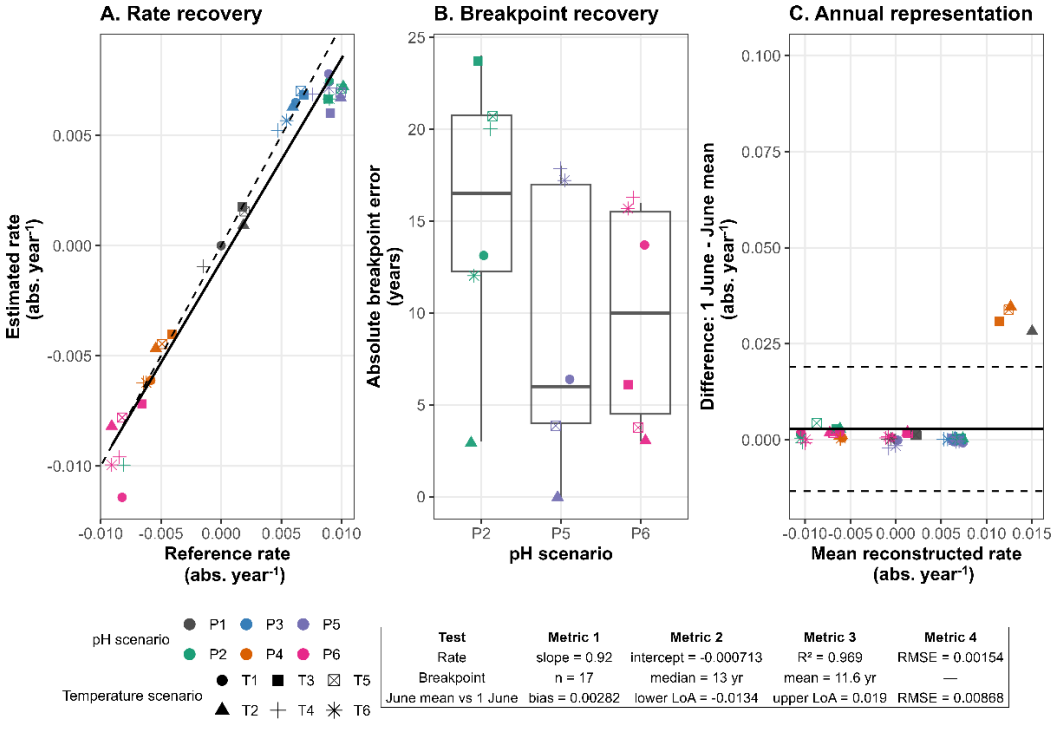

370

Figure 5. Validation of the segmentation framework showing (A) agreement between estimated and reference biological rates, (B) breakpoint estimation error, and (C) comparison of annual aggregation methods.

https://doi.org/10.5194/egusphere-2026-4577
Preprint. Discussion started: 20 August 2026

The framework estimated breakpoint with lower precision than biotic rates (Fig. 5b). Across the 17 segmented trajectories, the median absolute breakpoint error was 13 years (mean = 11.6 years, Table A2), corresponding to 12% of 108 years analysis window. Breakpoint errors varied among response trajectories and were largest for pronounced hump-shaped and threshold responses, whereas response trajectories with a smaller difference between the pre- and post-breakpoint slopes generally showed smaller breakpoint errors.

The choice of annual representation had little influence on estimated biotic rates (Fig. 5c). Rates based on performance on 1 June closely agreed with those based on mean June performance. The mean difference between the two representations was 0.003, and the RMSE was 0.009 (Table A2). Most differences clustered around zero, while larger deviations were limited to a few trajectories with the strongest positive rates. Under the tested simulation conditions, the fixed-date annual representation therefore produced long-term rate estimates like those obtained using the June-mean representation.

4.3 Cross-station transferability

Estimated rates of segmented biological trajectories showed broadly similar patterns across the four site-specific abiotic transitions, although their magnitudes varied among sites (Fig. 6). For the cases with the neutral temperature response (T1), the monotonic increasing and decreasing phases generated by T1-P3 and T1-P4 remained clearly distinct across all sites. The hump-shaped combination T1-P2 produced increasing and declining phases on opposite sides of its optimum, whereas the threshold-like combinations T1-P5 and T1-P6 produced a changing phase and a near-zero plateau phase.

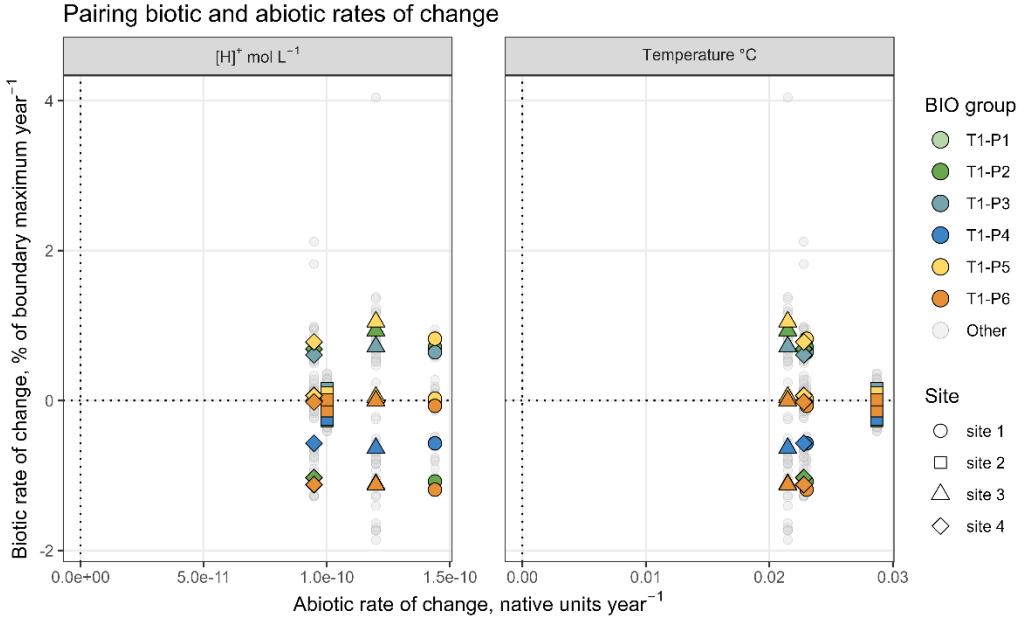

Figure 6. Biotic rates of change paired with full-period abiotic rates (temperature in °C and [H^+] in mol L^{-1}) across four simulated sites. The colour key highlights only trajectories with fixed neutral temperature-performance function in combination with six variants of pH-performance functions, similar as in Figure 4.

https://doi.org/10.5194/egusphere-2026-4577
Preprint. Discussion started: 20 August 2026

Across all 36 joint temperature-pH biological response trajectories, the ranking of estimated segment rates was largely preserved among sites (Spearman's $\rho = 0.66$ - 0.95; Table A3). Rank correlation was highest between Sites 1 and 3 ($\rho = 0.95$, $p < 0.001$) and lowest between Sites 1 and 2 ($\rho = 0.66$, $p < 0.001$), indicating that most pH-specific responses retained a similar relative position despite site-specific differences in rate magnitude.

5. Discussion

5.1. Addressing distinct analytical requirements between biotic and abiotic time series

Monitoring combines two fundamentally different types of observations. Physicochemical variables generally evolve as continuous long-term trajectories that can be described using established trend-analysis approaches, whereas biological responses are often heterogeneous, nonlinear, and phase-dependent. The framework presented here addresses this asymmetry by combining continuous abiotic trend estimation with segmented biotic rate estimation, thereby operationalizing the conceptual framework proposed by Widdicombe et al. (2023). Rather than redefining OA methodologies, it integrates existing best practices for OA time series analysis (Sutton et al., 2022) with a standardized biotic workflow that enables direct comparison of biotic and abiotic rates of change. The following discussion considers the principal methodological decisions underlying this approach, their implications, and their current limitations.

5.2. Standardizing heterogeneous biological observations

Biological monitoring data remain highly heterogeneous despite ongoing international efforts toward standardization (Bayraktarov et al., 2019; Benson et al., 2022; Bowler et al., 2025; Grenié et al., 2023; Klein et al., 2019; Muller-Karger et al., 2018). Consequently, absolute values of biological indicators are often not directly comparable across monitoring programmes. Nevertheless, changes within these time series can be compared when each series is analysed consistently relative to its own scale (O'Brien et al., 2017). Building on the conceptual framework of Widdicombe et al. (2023), we therefore standardize observations into biological groups and traits and express responses as rates of relative biological change. This provides a common analytical framework for comparing heterogeneous biological indicators while preserving the ecological meaning of individual time series.

Standardization also requires a common temporal representation. The framework therefore represents each biotic time series by one standardized value per year, derived either annually or within a consistent seasonal sampling window. This approach is consistent with previous ecological monitoring studies that have used annual indices or anomalies to quantify long-term biological change (Brien et al., 2017; Fewster et al., 2000; Knape, 2016; Mackas et al., 2012, 2001; Yebra et al., 2022). However, this approach is appropriate only for variables that provide an ecologically meaningful long-term state indicator at that temporal resolution. Variables describing short-lived physiological responses, episodic events, or within-year timing should be excluded unless they can be converted into comparable annual indices.

https://doi.org/10.5194/egusphere-2026-4577
Preprint. Discussion started: 20 August 2026

Our validation showed that, within the tested simulated scenarios, rates estimated from performance on 1 June closely matched those derived from mean June performance. This demonstrates agreement between two annual representations within the same predefined seasonal window, not that one observation per year is generally sufficient. The appropriate temporal aggregation is likely to depend on the taxon, trait, ecological process, site, and seasonal dynamics and cannot necessarily be determined a priori. Higher-frequency observations are therefore required to characterize seasonal variability, identify and validate a representative sampling window, and detect changes in phenology or seasonal succession. A single standardized annual observation should be used for long-term rate estimation only when its biological representativeness has been established using ecological knowledge or higher-frequency data. This result concerns the analysis of existing low-frequency records and should not be interpreted as justification for reducing monitoring frequency.

5.3. Representing nonlinear biological response trajectories

A central challenge in biological rate-of-change analysis is that ecological trajectories are rarely monotonic. Linear regression and non-parametric approaches such as the seasonal Mann–Kendall test provide robust estimates of long-term monotonic trends (O'Brien et al., 2017; Hirsch et al., 1982). Despite this strength, these approaches may average across ecologically distinct response phases when biological trajectories exhibit delayed responses, abrupt transitions, or regime shifts driven by interacting environmental and ecological processes (Andersen et al., 2009; Bode, 2024; Conversi et al., 2015; deYoung et al., 2008).

Flexible approaches such as Generalized Additive Models (GAMs) and Generalized Additive Mixed Models (GAMMs) reconstruct complex nonlinear trajectories and identify periods of changing response (Fewster et al., 2000; Knape, 2016; Simpson, 2018). However, because these models produce continuously varying slopes, they do not naturally yield a single biological rate that can be directly compared with physicochemical change over the same period.

Pairwise regression provides an alternative by partitioning trajectories into locally linear phases separated by estimated breakpoints (Muggeo, 2003; Tomal and Ciborowski, 2020; Toms and Lesperance, 2003). Our implementation adopts this general philosophy but is designed specifically to estimate comparable biotic and abiotic rates of change rather than to reconstruct complete ecological trajectories. By selecting the simplest representation supported by the data, the framework preserves the dominant structure of biological responses while producing standardized segment-specific rates that can be paired directly with continuous abiotic trends. We deliberately restricted the analysis to a single breakpoint, reflecting the primary objective of identifying comparable long-term rates rather than resolving every ecological transition.

5.4. Validation of the framework

The validation of the workflow performance demonstrated that a simplified one-breakpoint representation was sufficient to estimate the dominant biological rates of change across a broad range of simulated biological response trajectories. Despite stochastic variability and nonlinear ecological trajectories, estimated biological rates closely matched the reference rates, indicating that the framework retained the information required for biological-OA rate comparisons.

https://doi.org/10.5194/egusphere-2026-4577
Preprint. Discussion started: 20 August 2026

Importantly, rate estimates were considerably more accurate than breakpoint-location estimates. This behaviour is expected because segmented regression generally estimates slopes more robustly than breakpoint positions, particularly when several neighbouring breakpoints produce similarly good model fits (Muggeo, 2003; Toms and Lesperance, 2003). Under these conditions, different breakpoint locations may yield nearly identical segment slopes, making breakpoint timing inherently less identifiable than the associated rates of change. Consequently, accurate estimation of segment-specific rates is more important for comparative rate analysis than precise identification of the breakpoint year.

5.5. Controlled validation using response surfaces

The framework validation was based on biological response trajectories generated from simplified temperature-pH biological response surfaces. We adopted a multiplicative formulation because it provides a simple, internally consistent representation of co-limitation and enables systematic evaluation across a broad range of predefined response trajectories. Similar multiplicative formulations are widely used in ecological and biogeochemical models (De Groot, 1983; Poggiale et al., 2010; Shearer et al., 2015; Vadas and Orth, 2001). We do not suggest that biological responses to OA and warming are generally multiplicative. The effects of multiple physicochemical drivers on biological responses are often additive, antagonistic, synergistic, or otherwise nonlinear, depending on the species, biological process, and environmental context (Diamant et al., 2023; Rynkowski et al., 2025). The objective of the simulations was therefore not to reproduce ecological mechanisms, but to provide controlled and interpretable trajectories for evaluating the performance of the analytical framework. The simulations test performance under known, biologically plausible trajectory structures, but do not represent the full complexity or range of rates encountered in natural systems. Application to observed biological and carbonate chemistry time series is the next stage of framework evaluation.

5.6. Uncertainty in segmented trajectory reconstruction

Trajectory estimation revealed a systematic reduction in the accuracy of secondary segment slopes, particularly in threshold-type responses. Although the dominant ecological transition was consistently preserved, post-breakpoint trends were reconstructed less accurately than the corresponding pre-breakpoint trends. This pattern was supported by significantly larger slope errors for the second segment than for the first (Wilcoxon test, $p = 0.023$; Table A4).

Because breakpoint location and segment slopes are estimated jointly, the uncertainty in breakpoint estimation inevitably contributes to the uncertainty in the estimated slopes (Bellman and Roth, 1969; Guthery, 1974; Muggeo, 2003). Within our simulations, however, the secondary slope error could not be explained by the breakpoint error, segment duration, expected slope magnitude, slope contrast, or the number of observations assigned to the reconstructed segment (Table A4). Instead, the results suggest an inherent limitation of segmented regression under realistic observational variability, whereby the uncertainty associated with estimating the breakpoint disproportionately affects the following segment.

Consequently, estimated breakpoints should be interpreted as approximations of the dominant ecological transition period rather than precise biological tipping points (Andersen et al., 2009; Toms and Lesperance, 2003). Incorporating confidence

https://doi.org/10.5194/egusphere-2026-4577
Preprint. Discussion started: 20 August 2026

intervals around breakpoint estimates represents a logical extension of future versions of the framework (Muggeo, 2017; Tomal and Ciborowski, 2020).

5.7. Comparability across biological groups

Marine ecosystems are not closed systems and long-term biological time series frequently include genuine appearance and disappearance events that should be retained rather than treated as missing observations (Blasco-Moreno et al., 2019; Dumelle et al., 2025). Such trajectories create a mathematical difficulty for relative-change metrics because proportional change is undefined when the initial value is zero.

Existing transformations, including relative abundances, log-ratio methods, Hellinger transformation, and presence-absence approaches, were primarily developed for compositional analyses or to satisfy statistical assumptions rather than to estimate comparable rates of biological change (Bellier, 2012; Egozcue et al., 2003; Legendre and Gallagher, 2001). Min-max normalization is one of most prevalent scale normalizing approaches used in time series preprocessing (Asesh, 2022). Ranking each change relative to its observed maximum preserves ecologically meaningful appearance and disappearance events while producing bounded, directly comparable biological rates across heterogeneous indicators.

5.8. Transferability across abiotic trajectories

A major objective of the framework is to enable comparisons among time series experiencing different environmental histories (Widdicombe et al., 2023). Despite contrasting long-term abiotic transitions, the relative ordering of reconstructed biological responses remained largely preserved. This indicates that the framework captures general properties shared among the predefined biological response trajectories rather than features specific to individual abiotic trajectories. The preservation of response ranking is particularly important because comparative ecological studies primarily seek to identify the relative sensitivity of biological indicators across systems rather than reproduce identical response magnitudes. These results therefore support the application of the framework to cross-site comparisons and regional syntheses while recognizing that local physicochemical conditions will continue to influence the absolute magnitude of biological change.

5.9. Temporal coherence and casual inference

The proposed workflow is designed to assess whether long-term biological trajectories are temporally consistent with physicochemical changes, primarely in carbonate chemistry. Temporal coherence alone cannot establish that OA caused an observed biological response because marine ecosystems are influenced by multiple interacting drivers, including temperature, nutrient availability, circulation, species interactions, and other anthropogenic pressures. Consequently, correspondence between biological and carbonate chemistry rates should be interpreted as evidence of temporal coherence rather than causal attribution. Establishing causal relationships will continue to require complementary experimental studies, mechanistic understanding, and multivariate analyses that explicitly account for interacting physicochemical drivers.

https://doi.org/10.5194/egusphere-2026-4577
Preprint. Discussion started: 20 August 2026

5.10. Implications for OA monitoring

By translating heterogeneous biological datasets into standardized rate estimates, the workflow facilitates comparison among taxa, ecosystems, and monitoring programmes while preserving the ecological interpretation of individual biological indicators. The methodology therefore provides a practical tool for the Global Ocean Acidification Observing Network (GOA-ON), national monitoring programmes, and long-term ecological observatories seeking to evaluate candidate biological indicators of OA. More broadly, the analytical framework may also support investigations of other climate-driven stressors in which continuous forcing is coupled with nonlinear biological responses.

5.11. Future developments

Future developments should focus on extending the framework to more complex ecological trajectories, incorporating formal uncertainty estimates for breakpoint location and biological rates, evaluating multi-breakpoint representations were supported by data availability, and testing the workflow across diverse observational time series and ecosystems. Such applications will determine the extent to which standardized biological rates of change improve understanding of large-scale ecological responses to OA.

6. Conclusions

Controlled simulation experiments demonstrated that the proposed methodology can estimate dominant biological rates and transitions across the tested response trajectories. These results establish a proof of concept under known and interpretable conditions. The next step is to evaluate the empirical performance and broader applicability of the workflow using observed biological and carbonate chemistry time series. Namely, this new method will allow direct identification and comparison of the rates of change for potential abiotic explanatory variables, OA and beyond, and a suite of potential biological responses to that change. This methodology will now enable the conceptual framework proposed in the Widdicombe et al. (2023) to be applied to existing and emerging time series, and thereby further tested against a wide range of real-world observations. The growing number of OA time series established through capacity development supporting Sustainable Development Goal 14.3.1 indicator reporting and GOA-ON will further broaden the geographic scope and applicability of the framework, particularly in historically underrepresented regions. As applications accumulate, comparisons across systems will provide new evidence about the contribution of OA to observed biological change and the conditions that moderate or exacerbate its effects. This growing context-specific knowledge can support more effective observation, management, and mitigation of the causes and consequences of OA for marine communities and biodiversity.

https://doi.org/10.5194/egusphere-2026-4577
Preprint. Discussion started: 20 August 2026

Appendix A

Table A1. Definition of the six trapezoid performance (T/P) functions applied separately to temperature and pH. The lower and upper zero-performance limits were defined by extending the full modelled June range by 30% at both ends. Optimal plateau boundaries were positioned relative to the modelled abiotic transition window between the mean conditions during the first and last 10 years of the simulation.

T/P	Response type	$X_{low,0}$	$X_{opt,min}$	$X_{opt,max}$	$X_{high,0}$	Description
1	Flat (no response)	X_{min}-0.3R	X_{min}	X_{max}	X_{max} +0.3R	Maximum performance across the full observed OA range.
2	Hump-shaped	X_{min} -0.3R	X_{mid} -0.10W	X_{mid} +0.10W	X_{max} +0.3R	Narrow optimum centered on the transition midpoint.
3	Positive	X_{min} -0.3R	X_{max} -0.05W	X_{max}	X_{max} +0.3R	Performance increases throughout the OA transition.
4	Negative	X_{min} -0.3R	X_{min}	X_{min} +0.05W	X_{max} +0.3R	Performance decreases throughout the OA transition.
5	Threshold-positive	X_{min} -0.3R	X_{mid}	X_{max}	X_{max} +0.3R	Abrupt increase after the transition midpoint.
6	Threshold-negative	X_{min} -0.3R	X_{min}	X_{mid}	X_{max} +0.3R	Abrupt decrease after the transition midpoint.

where:

$X_{low,0}$ – the lower zero-performance limit

$X_{opt,min}$ – the lower optimal plateau bound

$X_{opt,max}$ – the upper optimal plateau bound

$X_{high,0}$ – the upper zero-performance limit

X_{min} – is the minimum observed June value over the full simulation

X_{min} – is the maximum observed June value over the full simulation

X_{start} – is the mean June value during the first 10 simulation years

X_{end} – is the mean June value during the last 10 simulation years

$R = X_{max} - X_{min}$ – is the full observed June abiotic range

$W = |X_{end} - X_{start}|$ – is the abiotic transition window

$X_{mid} = (X_{start} + X_{end})/2$ – is the transition window middle point

https://doi.org/10.5194/egusphere-2026-4577
Preprint. Discussion started: 20 August 2026

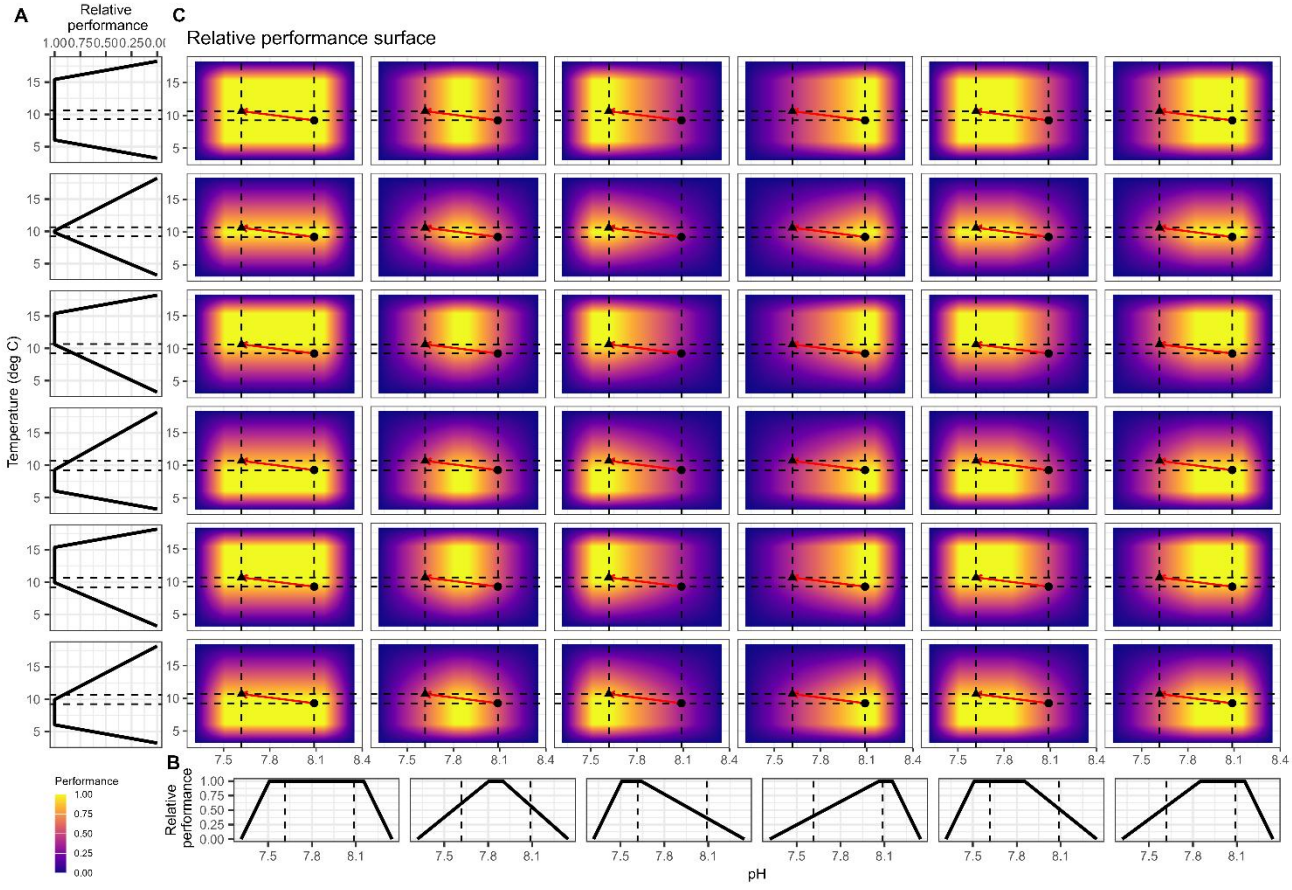

Figure A1. Definition of simplified trapezoid (A) temperature- and (B) pH-specific performance functions and resulting (C) combined performance surfaces of biological response. Each red arrow represents an abiotic transition from initial temperature-pH conditions (black circle) to final conditions (black triangle). The six surfaces in the top row, combining T1 with P1-P6, are developed further in Figure 4.

https://doi.org/10.5194/egusphere-2026-4577
Preprint. Discussion started: 20 August 2026

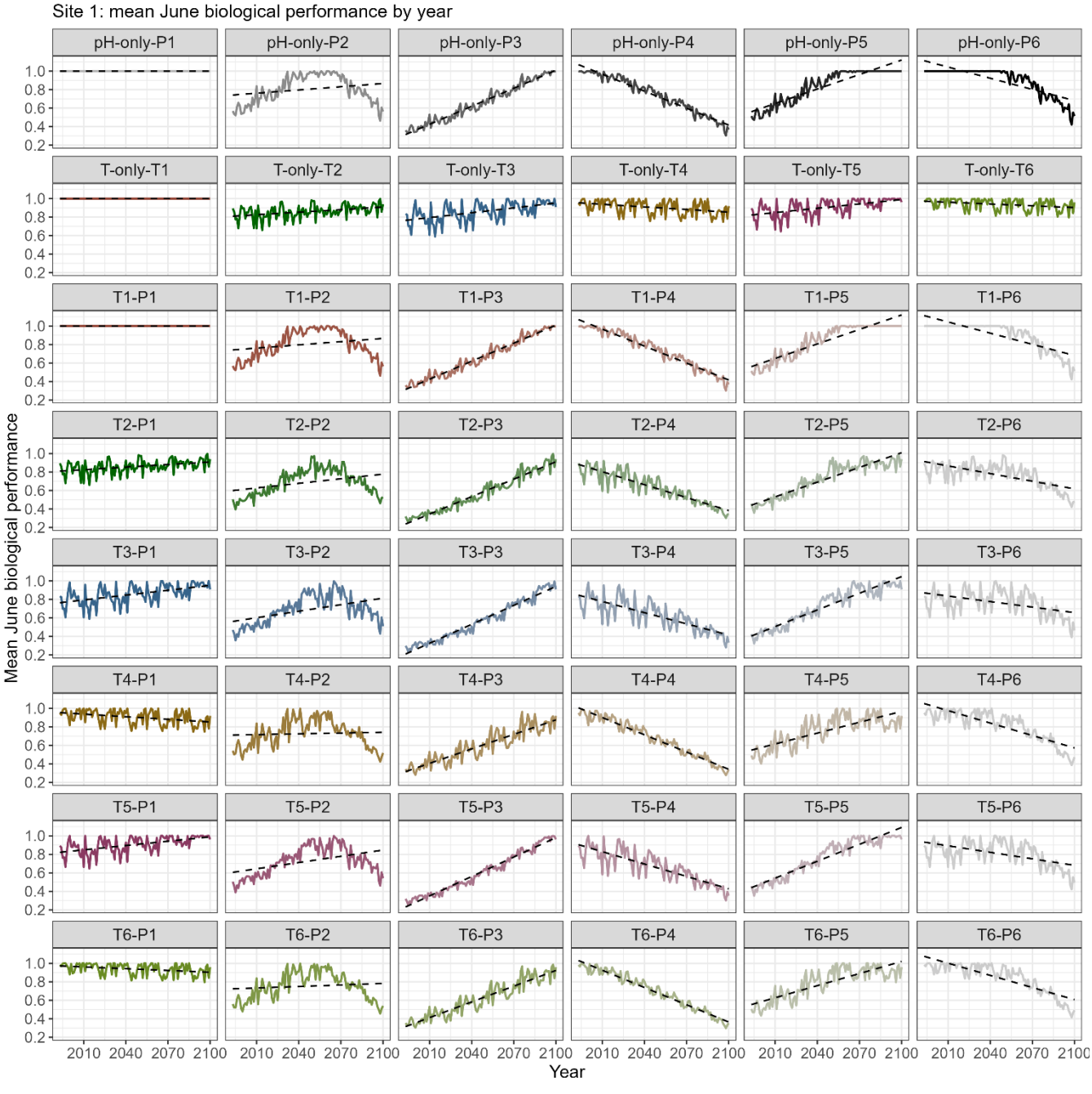

Figure A2. Simulated biotic time series for 36 defined biological response trajectories. Dashed lines indicate linear regressions fitted separately to each trajectory.

https://doi.org/10.5194/egusphere-2026-4577
Preprint. Discussion started: 20 August 2026

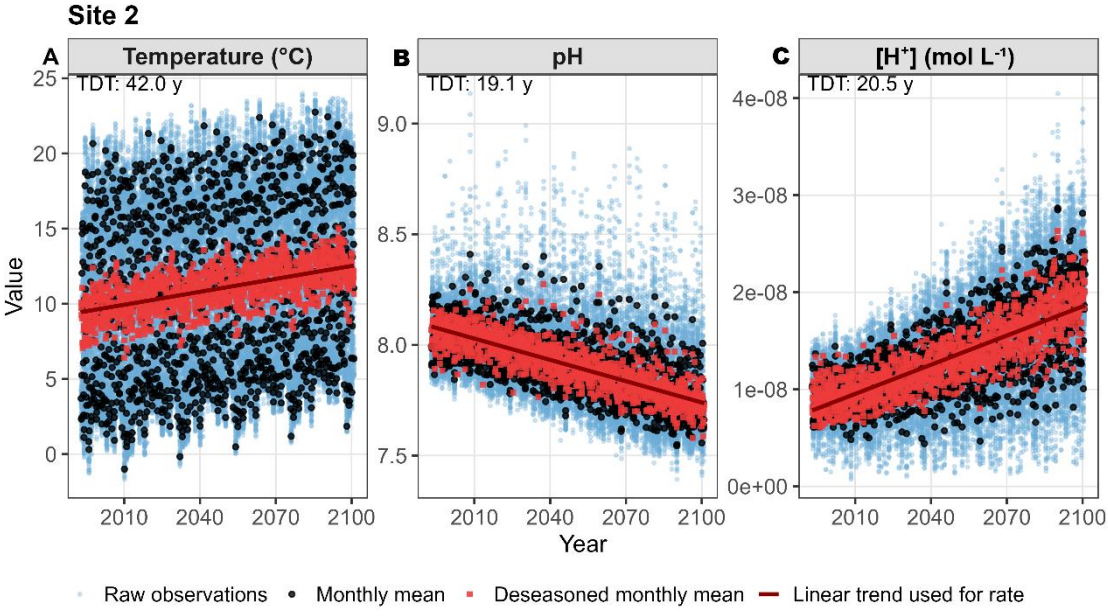

Figure A3. Deseasoned long-term trajectories of (A) temperature (°C), (B) hydrogen ion concentration ([H^+], mol L^{-1}), and (C) pH at Site 2 for 1993-2100. Light-blue points show the original model output, black points show monthly means, and red points show the corresponding deseasoned monthly mean values. Solid dark red lines represent the estimated long-term trend. The trend detection time (TDT) is represented in years.

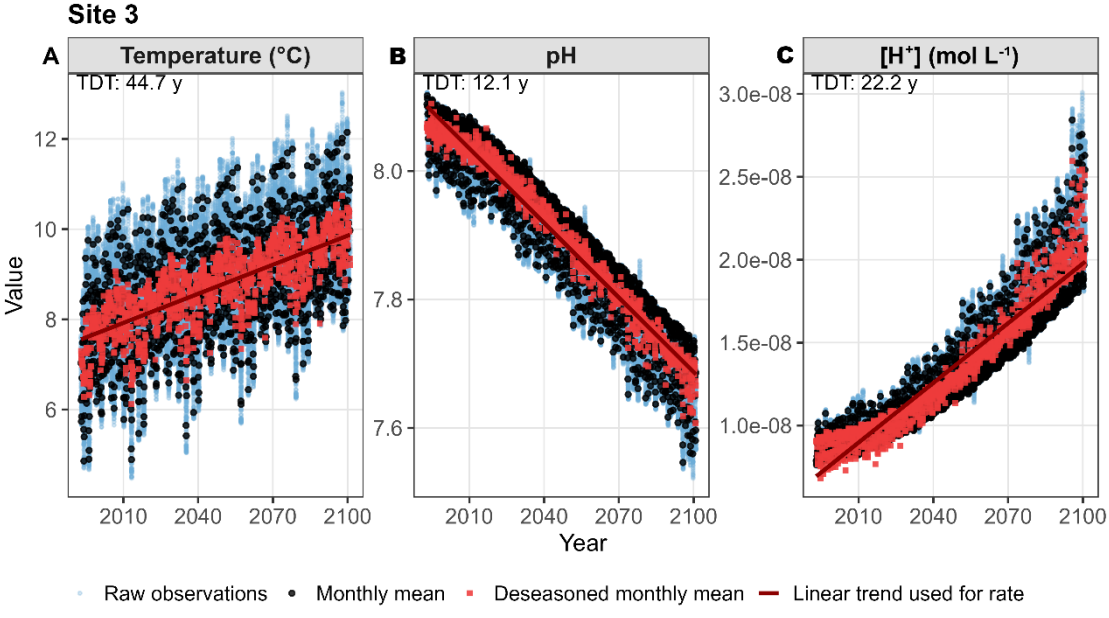

Figure A4. Deseasoned long-term trajectories of (A) temperature (°C), (B) hydrogen ion concentration ([H^+], mol L^{-1}), and (C) pH at Site 3 for 1993-2100. Light-blue points show the original model output, black points show monthly means, and red points show the corresponding deseasoned monthly mean values. Solid dark red lines represent the estimated long-term trend. The trend detection time (TDT) is represented in years.

https://doi.org/10.5194/egusphere-2026-4577
Preprint. Discussion started: 20 August 2026

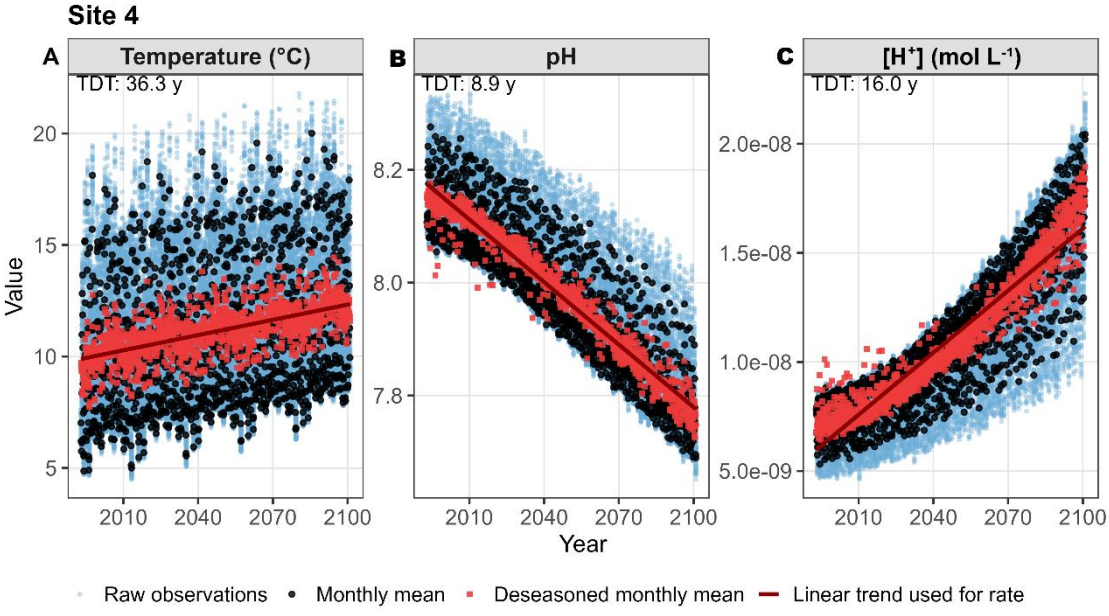

Figure A5. Deseasoned long-term trajectories of (A) temperature (°C), (B) hydrogen ion concentration ([H^+], mol L^{-1}), and (C) pH at Site 4 for 1993-2100. Light-blue points show the original model output, black points show monthly means, and red points show the corresponding deseasoned monthly mean values. Solid dark red lines represent the estimated long-term trend. The trend detection time (TDT) is represented in years.

https://doi.org/10.5194/egusphere-2026-4577
Preprint. Discussion started: 20 August 2026

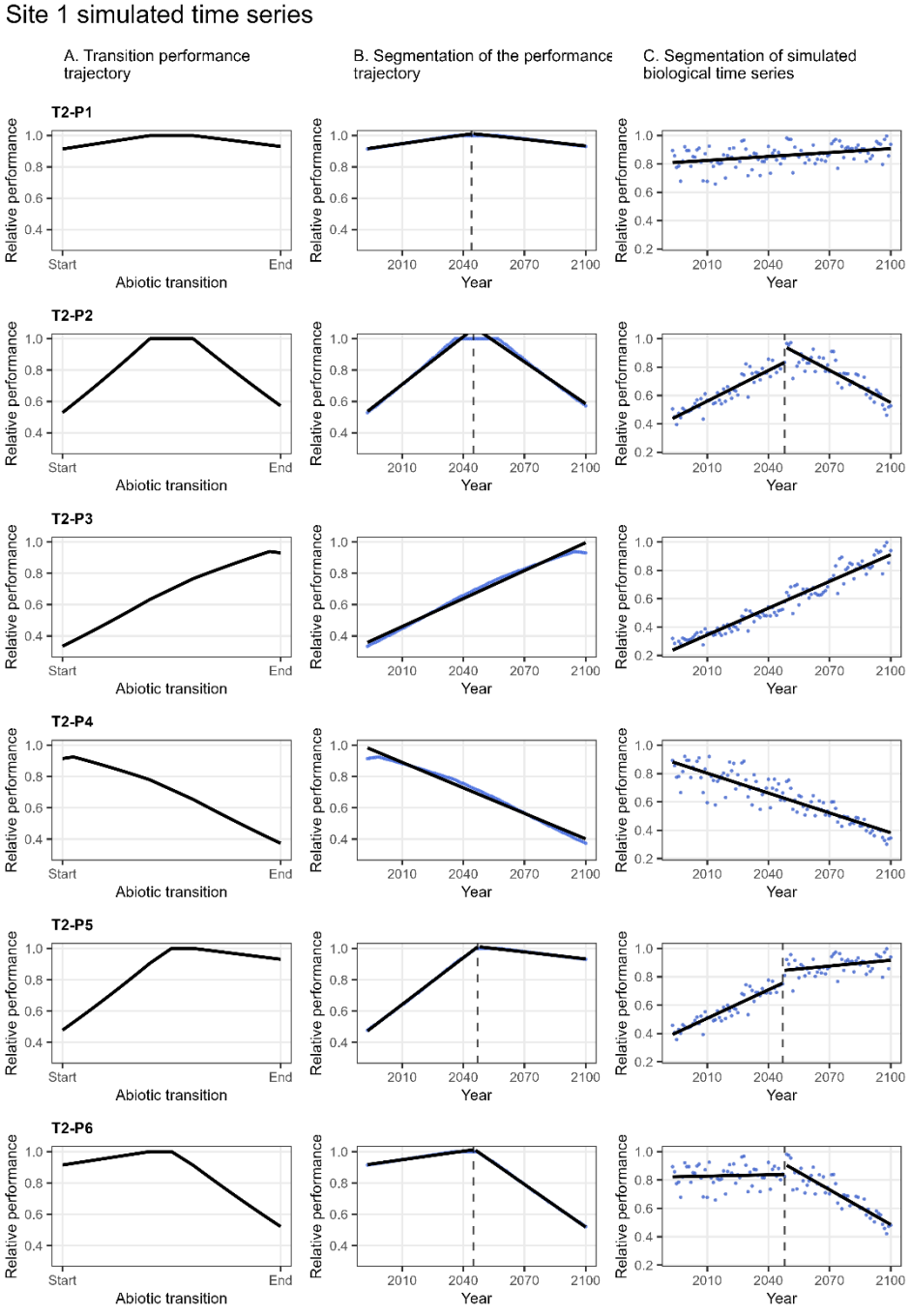

Figure A6. Translation of temperature-pH performance surfaces into simulated biological trajectories and segmented fits at Site 1. The six rows combine the hump-shaped temperature-response function (T2) with the six pH-response functions (P1-P6) and correspond to the six surfaces in the second row of Figure A1. (A) The left column shows the reference performance profile along the Site 1 start-to-end temperature-pH transition path shown in Figure A1. (B) The middle column shows the resulting noise-free temporal trajectory (blue) and its fitted linear or one-breakpoint model (black). (C) The right column shows the corresponding noise-added simulated biological time series (blue) and fitted model (black). Vertical dashed lines indicate estimated breakpoints.

https://doi.org/10.5194/egusphere-2026-4577
Preprint. Discussion started: 20 August 2026

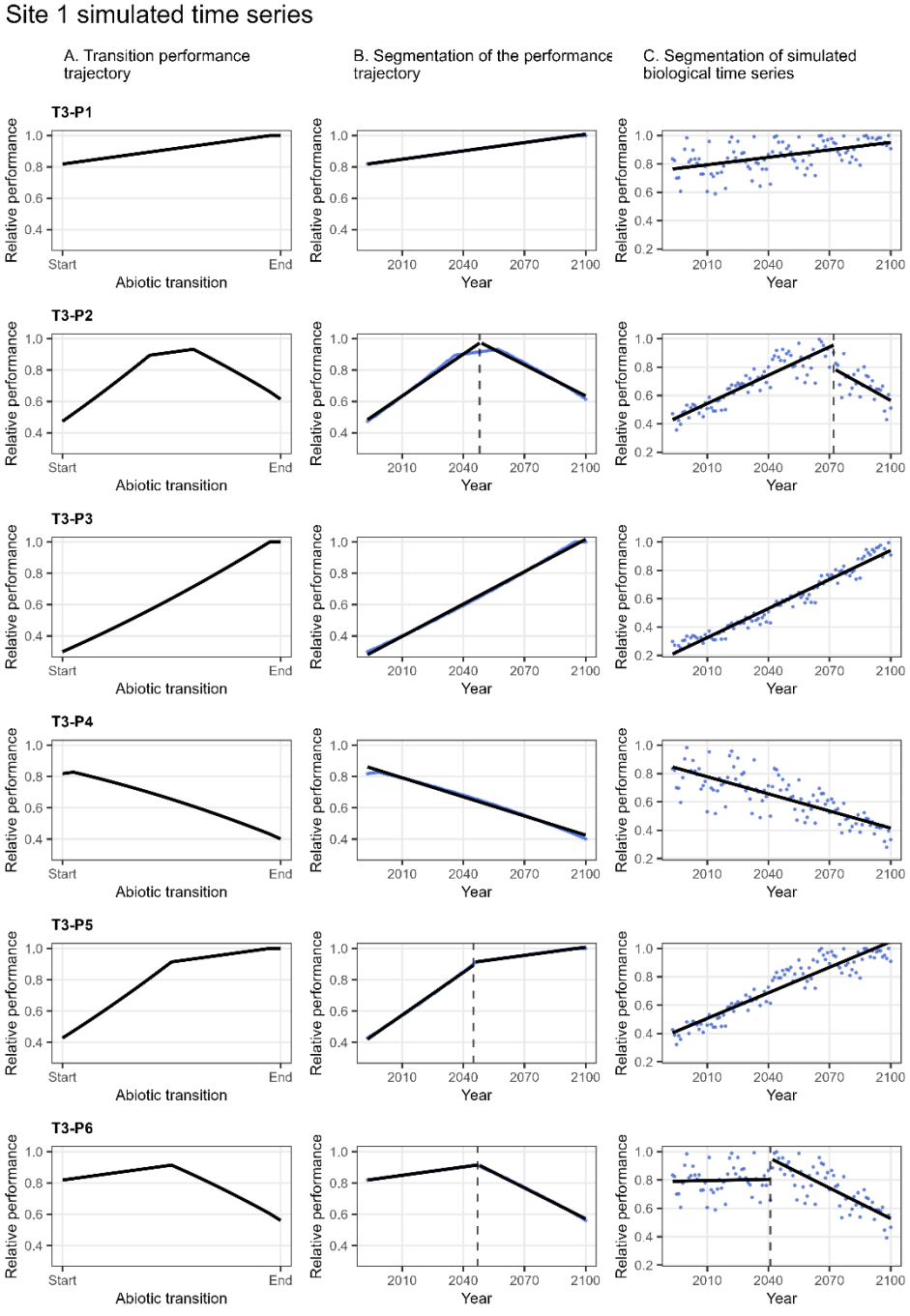

Figure A7. Translation of temperature-pH performance surfaces into simulated biological trajectories and segmented fits at Site 1. **The six rows combine the positive temperature-response function (T3) with the six pH-response functions (P1-P6) and correspond to the six surfaces in the third row of Figure A1. (A) The left column shows the reference performance profile along the Site 1 start-to-end temperature-pH transition path shown in Figure A1. (B) The middle column shows the resulting noise-free temporal trajectory (blue) and its fitted linear or one-breakpoint model (black). (C) The right column shows the corresponding noise-added simulated biological time series (blue) and fitted model (black). Vertical dashed lines indicate estimated breakpoints.**

https://doi.org/10.5194/egusphere-2026-4577
Preprint. Discussion started: 20 August 2026

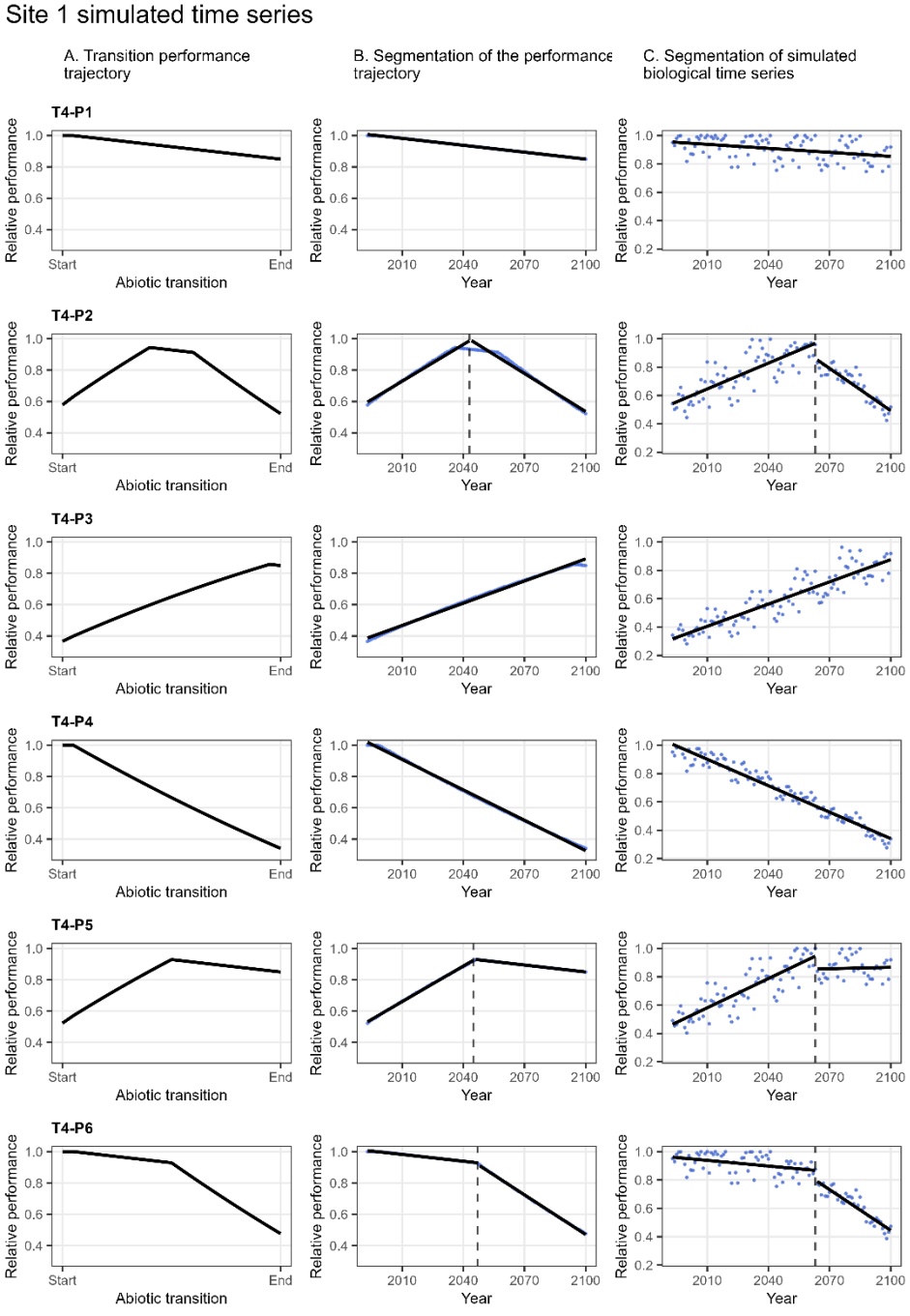

Figure A8. Translation of temperature-pH performance surfaces into simulated biological trajectories and segmented fits at Site 1. The six rows combine the negative temperature-response function (T4) with the six pH-response functions (P1-P6) and correspond to the six surfaces in the fourth row of Figure A1. (A) The left column shows the reference performance profile along the Site 1 start-to-end temperature-pH transition path shown in Figure A1. (B) The middle column shows the resulting noise-free temporal trajectory (blue) and its fitted linear or one-breakpoint model (black). (C) The right column shows the corresponding noise-added simulated biological time series (blue) and fitted model (black). Vertical dashed lines indicate estimated breakpoints.

https://doi.org/10.5194/egusphere-2026-4577
Preprint. Discussion started: 20 August 2026

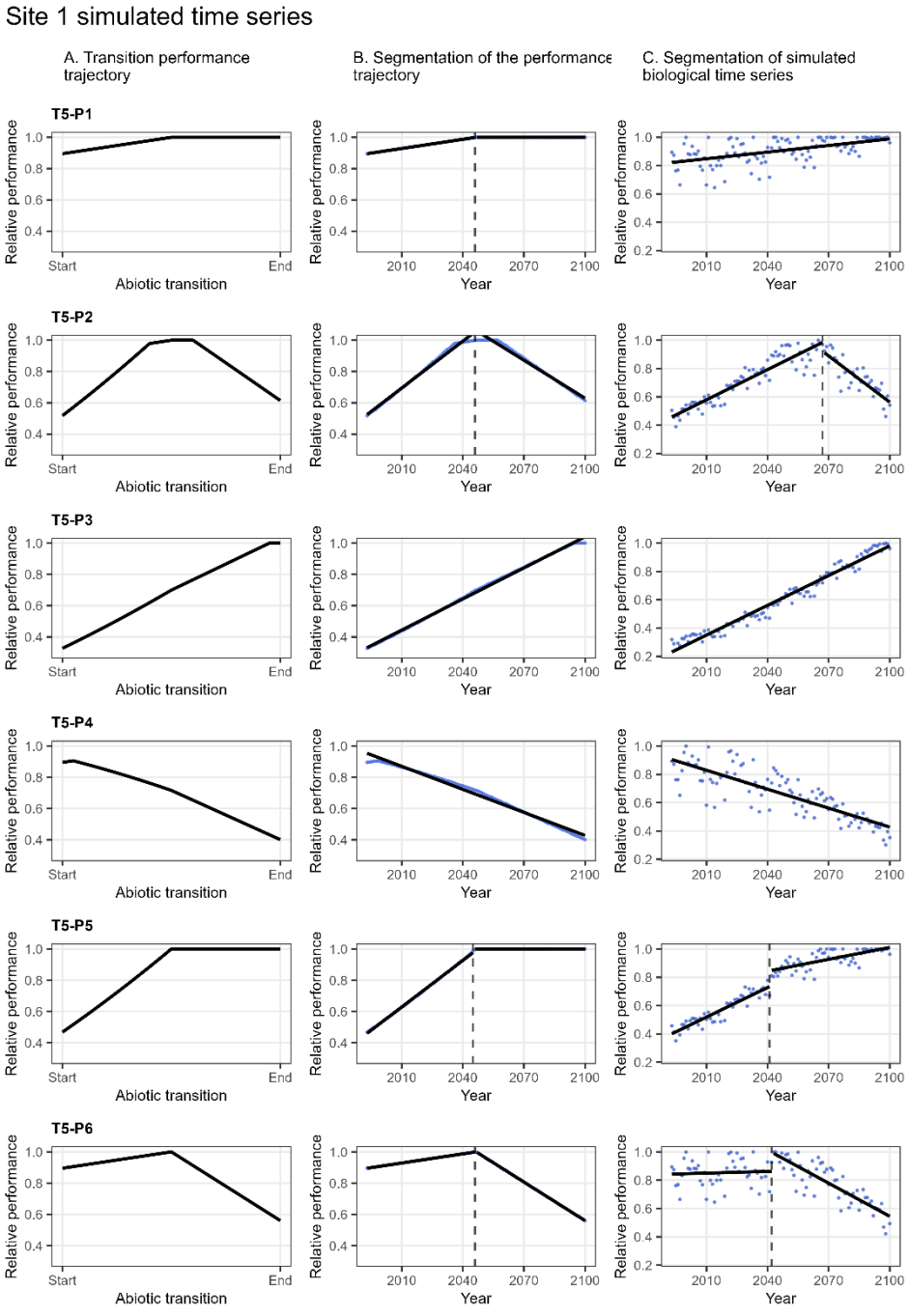

Figure A9. Translation of temperature-pH performance surfaces into simulated biological trajectories and segmented fits at Site 1. The six rows combine the threshold-positive temperature-response function (T5) with the six pH-response functions (P1-P6) and correspond to the six surfaces in the fifth row of Figure A1. (A) The left column shows the reference performance profile along the Site 1 start-to-end temperature-pH transition path shown in Figure A1. (B) The middle column shows the resulting noise-free temporal trajectory (blue) and its fitted linear or one-breakpoint model (black). (C) The right column shows the corresponding noise-added simulated biological time series (blue) and fitted model (black). Vertical dashed lines indicate estimated breakpoints.

https://doi.org/10.5194/egusphere-2026-4577
Preprint. Discussion started: 20 August 2026

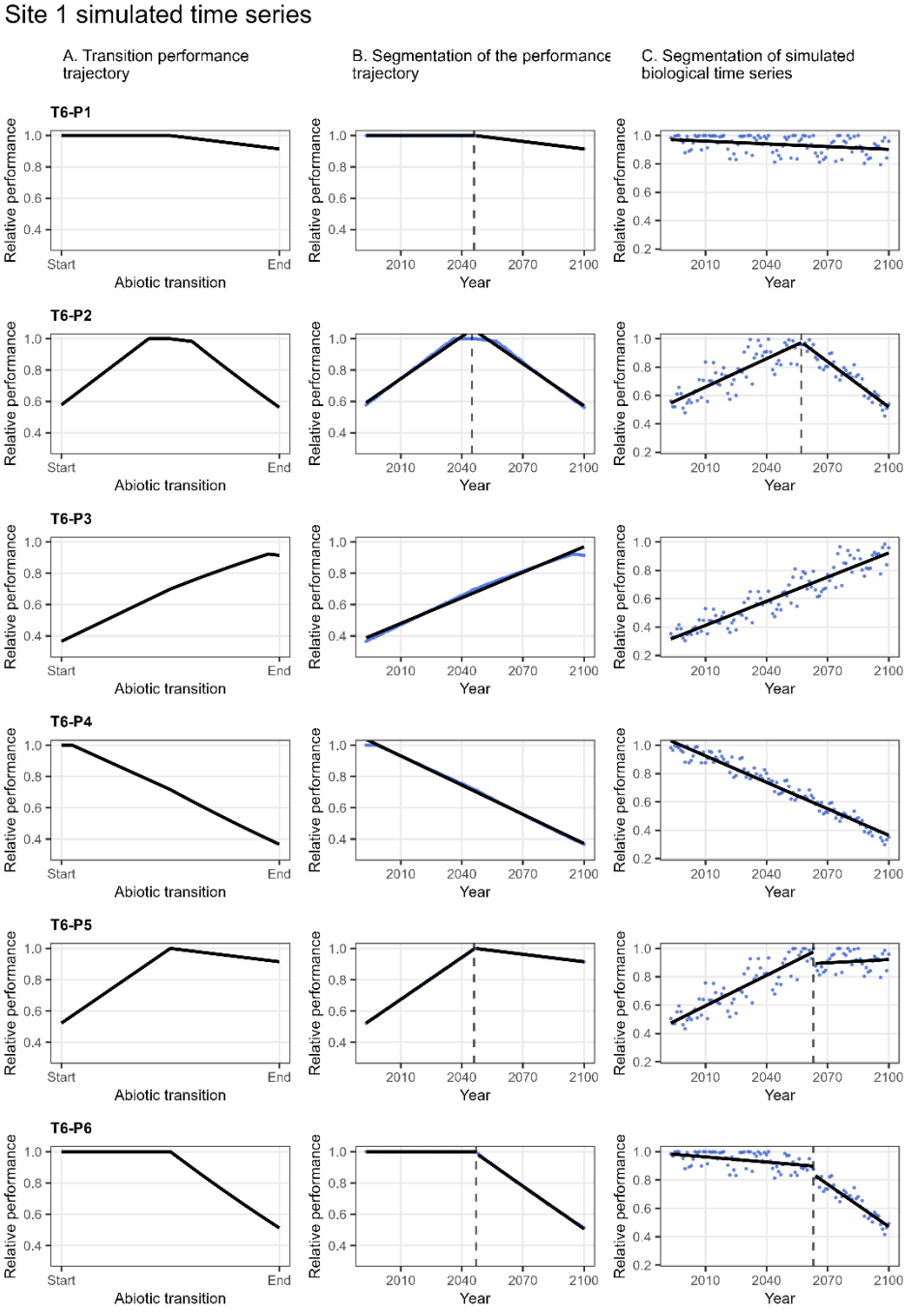

615 **Figure A10. Translation of temperature-pH performance surfaces into simulated biological trajectories and segmented fits at Site 1. The six rows combine the threshold-negative temperature-response function (T6) with the six pH-response functions (P1-P6) and correspond to the six surfaces in the sixth row of Figure A1. (A) The left column shows the reference performance profile along the Site 1 start-to-end temperature-pH transition path shown in Figure A1. (B) The middle column shows the resulting noise-free temporal trajectory (blue) and its fitted linear or one-breakpoint model (black). (C) The right column shows the**

https://doi.org/10.5194/egusphere-2026-4577
Preprint. Discussion started: 20 August 2026

corresponding noise-added simulated biological time series (blue) and fitted model (black).Vertical dashed lines indicate estimated breakpoints.

Table A2. Summary statistics describing framework validation performance.

	Nr of observations	Intercept	Slope	R^2	RMSE
Agreement between estimated and reference rates	35	-0.0007	0.9202	0.96	0.0015

	Nr of breakpoints	Median absolute breakpoint error	Mean absolute breakpoint error
Breakpoint estimation error	17	13	11.58

	Nr of observations	bias	SD difference	Lower limit	Upper limit	RMSE
Bland-Altman summary	66	0.0028	0.0082	-0.0134	0.0190	0.0086

Table A2. Pairwise Spearman rank correlations of reconstructed biological response rankings among simulated sites.

Site	site 1	site 2	site 3	site 4
site 1	—	0.66	0.95	0.86
site 2	<0.001	—	0.83	0.84
site 3	<0.001	<0.001	—	0.82
site 4	<0.001	<0.001	<0.001	—

Table A3. Statistical evaluation of potential causes of reduced accuracy in secondary segment slope estimation.

Question	Test	Statistic	p-value	Interpretation
Is slope error larger in Segment 2 than Segment 1?	Wilcoxon rank-sum test	W = 187	0.023	Segment 2 had significantly larger slope error.
Is Segment 2 slope error related to breakpoint error?	Spearman correlation	ρ = 0.203	0.435	No evidence that breakpoint error explained Segment 2 slope error.
Is Segment 2 slope error related to expected Segment 2 slope magnitude?	Spearman correlation	ρ = -0.216	0.405	No evidence that expected slope magnitude explained Segment 2 slope error.

https://doi.org/10.5194/egusphere-2026-4577
Preprint. Discussion started: 20 August 2026

Is Segment 2 slope error related to expected slope contrast between segments?	Spearman correlation	$\rho = 0.326$	0.202	No evidence that slope contrast explained Segment 2 slope error.
Is segmented biological time series vs segmented performance trajectory slope difference larger in Segment 2 than Segment 1?	Wilcoxon rank-sum test	$W = 187$	0.023	Noisy trajectories produced larger slope differences in Segment 2.

Code and data availability

The R workflow implementing the rate-of-change framework is freely available from the project's GitHub repository (https://github.com/OAPoCfNRS/RoC-tool). The modelled temperature and pH time series used to derive the threshold parameters and generate the simulated biological response trajectories were provided by Yuri Artioli and are available upon request.

Author contributions

Conceptualization: NS, SW, SD, KI, PH; methodology: NS, SW, SD, KI, PH; data curation: NS, YA; formal analysis, visualization and original draft preparation: NS; review and editing: NS, SW, SD, KI, PH, YA, HE; funding acquisition: HE.

Competing interests

The contact author has declared that neither of the authors has any competing interests.

Disclaimer

Copernicus Publications remains neutral with regard to jurisdictional claims made in the text, published maps, institutional affiliations, or any other geographical representation in this paper. While Copernicus Publications makes every effort to

https://doi.org/10.5194/egusphere-2026-4577
Preprint. Discussion started: 20 August 2026

include appropriate place names, the final responsibility lies with the authors. Views expressed in the text are those of the authors and do not necessarily reflect the views of the publisher.

Acknowledgements

We thank the Intergovernmental Oceanographic Commission of UNESCO and the Velux Foundation for the financial support. We further thank the GOA-ON biological working group for the guidance provided.

Financial support

Velux Foundation Project 00063479 via the Intergovernmental Oceanographic Commission of UNESCO.

References

Andersen, T., Carstensen, J., Hernández-García, E., Duarte, C.M., 2009. Ecological thresholds and regime shifts: approaches to identification. Trends in Ecology & Evolution 24, 49–57. https://doi.org/10.1016/j.tree.2008.07.014

Asesh, A., 2022. Normalization and Bias in Time Series Data, in: Biele, C., Kacprzyk, J., Kopeć, W., Owsiński, J.W., Romanowski, A., Sikorski, M. (Eds.), Digital Interaction and Machine Intelligence, Lecture Notes in Networks and Systems. Springer International Publishing, Cham, pp. 88–97. https://doi.org/10.1007/978-3-031-11432-8_8

Bates, N., Astor, Y., Church, M., Currie, K., Dore, J., Gonaález-Dávila, M., Lorenzoni, L., Muller-Karger, F., Olafsson, J., Santa-Casiano, M., 2014. A Time-Series View of Changing Ocean Chemistry Due to Ocean Uptake of Anthropogenic CO2 and Ocean Acidification. oceanog 27, 126–141. https://doi.org/10.5670/oceanog.2014.16

Bates, N.R., 2001. Interannual variability of oceanic CO2 and biogeochemical properties in the Western North Atlantic subtropical gyre. Deep Sea Research Part II: Topical Studies in Oceanography 48, 1507–1528. https://doi.org/10.1016/S0967-0645(00)00151-X

Bayraktarov, E., Ehmke, G., O'Connor, J., Burns, E.L., Nguyen, H.A., McRae, L., Possingham, H.P., Lindenmayer, D.B., 2019. Do Big Unstructured Biodiversity Data Mean More Knowledge? Front. Ecol. Evol. 6, 239. https://doi.org/10.3389/fevo.2018.00239

Bednaršek, N., Feely, R.A., Howes, E.L., Hunt, B.P.V., Kessouri, F., León, P., Lischka, S., Maas, A.E., McLaughlin, K., Nezlin, N.P., Sutula, M., Weisberg, S.B., 2019. Systematic Review and Meta-Analysis Toward Synthesis of Thresholds of Ocean Acidification Impacts on Calcifying Pteropods and Interactions With Warming. Front. Mar. Sci. 6, 227. https://doi.org/10.3389/fmars.2019.00227

Bellier, E., 2012. D. Borcard, F. Gillet, P. Legendre: Numerical Ecology with R: Springer, New York, 2011. JABES 17, 308–309. https://doi.org/10.1007/s13253-012-0094-x

https://doi.org/10.5194/egusphere-2026-4577
Preprint. Discussion started: 20 August 2026

Bellman, R., Roth, R., 1969. Curve Fitting by Segmented Straight Lines. Journal of the American Statistical Association 64, 1079–1084. https://doi.org/10.1080/01621459.1969.10501038

Benson, A., LaScala-Gruenewald, D., McGuinn, R., Satterthwaite, E., Beaulieu, S., Biddle, M., deWitt, L., McKinzie, M., Montes, E., Moustahfid, H., Muller-Karger, F., Murray, T., Van de Putte, A., Cluster, E.B.D.S., 2022. Biological Observation Data Standardization - A Primer for Data Managers. https://doi.org/10.6084/M9.FIGSHARE.16806712

Bode, A., 2024. Synchronized multidecadal trends and regime shifts in North Atlantic plankton populations. ICES Journal of Marine Science 81, 575–586. https://doi.org/10.1093/icesjms/fsad095

Bowler, D.E., Boyd, R.J., Callaghan, C.T., Robinson, R.A., Isaac, N.J.B., Pocock, M.J.O., 2025. Treating gaps and biases in biodiversity data as a missing data problem. Biological Reviews 100, 50–67. https://doi.org/10.1111/brv.13127

Busch, D.S., McElhany, P., 2016. Estimates of the Direct Effect of Seawater pH on the Survival Rate of Species Groups in the California Current Ecosystem. PLoS ONE 11, e0160669. https://doi.org/10.1371/journal.pone.0160669

Butenschön, M., Clark, J., Aldridge, J.N., Allen, J.I., Artioli, Y., Blackford, J., Bruggeman, J., Cazenave, P., Ciavatta, S., Kay, S., Lessin, G., van Leeuwen, S., van der Molen, J., De Mora, L., Polimene, L., Sailley, S., Stephens, N., Torres, R., 2016. ERSEM 15.06: a generic model for marine biogeochemistry and the ecosystem dynamics of the lower trophic levels. Geosci. Model Dev. 9, 1293–1339. https://doi.org/10.5194/gmd-9-1293-2016

Canonico, G., Buttigieg, P.L., Montes, E., Muller-Karger, F.E., Stepien, C., Wright, D., Benson, A., Helmuth, B., Costello, M., Sousa-Pinto, I., Saeedi, H., Newton, J., Appeltans, W., Bednaršek, N., Bodrossy, L., Best, B.D., Brandt, A., Goodwin, K.D., Iken, K., Marques, A.C., Miloslavich, P., Ostrowski, M., Turner, W., Achterberg, E.P., Barry, T., Defeo, O., Bigatti, G., Henry, L.-A., Ramiro-Sánchez, B., Durán, P., Morato, T., Roberts, J.M., García-Alegre, A., Cuadrado, M.S., Murton, B., 2019. Global Observational Needs and Resources for Marine Biodiversity. Front. Mar. Sci. 6, 367. https://doi.org/10.3389/fmars.2019.00367

Carter, B.R., Williams, N.L., Evans, W., Fassbender, A.J., Barbero, L., Hauri, C., Feely, R.A., Sutton, A.J., 2019. Time of Detection as a Metric for Prioritizing Between Climate Observation Quality, Frequency, and Duration. Geophysical Research Letters 46, 3853–3861. https://doi.org/10.1029/2018GL080773

Conversi, A., Dakos, V., Gårdmark, A., Ling, S., Folke, C., Mumby, P.J., Greene, C., Edwards, M., Blenckner, T., Casini, M., Pershing, A., Möllmann, C., 2015. A holistic view of marine regime shifts. Phil. Trans. R. Soc. B 370, 20130279. https://doi.org/10.1098/rstb.2013.0279

De Groot, W.T., 1983. Modelling the multiple nutrient limitation of algal growth. Ecological Modelling 18, 99–119. https://doi.org/10.1016/0304-3800(83)90049-2

deYoung, B., Barange, M., Beaugrand, G., Harris, R., Perry, R.I., Scheffer, M., Werner, F., 2008. Regime shifts in marine ecosystems: detection, prediction and management. Trends in Ecology & Evolution 23, 402–409. https://doi.org/10.1016/j.tree.2008.03.008

https://doi.org/10.5194/egusphere-2026-4577
Preprint. Discussion started: 20 August 2026

Diamant, E.S., Boyd, S., Lozano-Huntelman, N.A., Enriquez, V., Kim, A.R., Savage, V.M., Yeh, P.J., 2023. Meta-analysis of three-stressor combinations on population-level fitness reveal substantial higher-order interactions. Science of The Total Environment 864, 161163. https://doi.org/10.1016/j.scitotenv.2022.161163

Dickson, A.G., Sabine, C.L., Christian, J.R., 2007. Guide to Best Practices for Ocean CO2 Measurements (No. 8), P I C E S S P E C I A L P U B L I C AT I O N. IOCCP.

Egozcue, J.J., Pawlowsky-Glahn, V., Mateu-Figueras, G., Barceló-Vidal, C., 2003. Isometric Logratio Transformations for Compositional Data Analysis. Mathematical Geology 35, 279–300. https://doi.org/10.1023/A:1023818214614

Fewster, R.M., Buckland, S.T., Siriwardena, G.M., Baillie, S.R., Wilson, J.D., 2000. ANALYSIS OF POPULATION TRENDS FOR FARMLAND BIRDS USING GENERALIZED ADDITIVE MODELS. Ecology 81, 1970–1984. https://doi.org/10.1890/0012-9658(2000)081%5B1970:AOPTFF%5D2.0.CO;2

Friedlingstein, P., O'Sullivan, M., Jones, M.W., Andrew, R.M., Bakker, D.C.E., Hauck, J., Landschützer, P., Le Quéré, C., Li, H., Luijkx, I.T., Peters, G.P., Peters, W., Pongratz, J., Schwingshackl, C., Sitch, S., Canadell, J.G., Ciais, P., Aas, K., Alin, S.R., Anthoni, P., Barbero, L., Bates, N.R., Bellouin, N., Benoit-Cattin, A., Berghoff, C.F., Bernardello, R., Bopp, L., Brasika, I.B.M., Chamberlain, M.A., Chandra, N., Chevallier, F., Chini, L.P., Collier, N.O., Colligan, T.H., Cronin, M., Djeutchouang, L.M., Dou, X., Enright, M.P., Enyo, K., Erb, M., Evans, W., Feely, R.A., Feng, L., Ford, D.J., Foster, A., Fransner, F., Gasser, T., Gehlen, M., Gkritzalis, T., Goncalves De Souza, J., Grassi, G., Gregor, L., Gruber, N., Guenet, B., Gürses, Ö., Harrington, K., Harris, I., Heinke, J., Hurtt, G.C., Iida, Y., Ilyina, T., Ito, A., Jacobson, A.R., Jain, A.K., Jarníková, T., Jersild, A., Jiang, F., Jones, S.D., Kato, E., Keeling, R.F., Klein Goldewijk, K., Knauer, J., Kong, Y., Korsbakken, J.I., Koven, C., Kunimitsu, T., Lan, X., Liu, J., Liu, Zhiqiang, Liu, Zhu, Lo Monaco, C., Ma, L., Marland, G., McGuire, P.C., McKinley, G.A., Melton, J.R., Monacci, N., Monier, E., Morgan, E.J., Munro, D.R., Müller, J.D., Nakaoka, S.-I., Nayagam, L.R., Niwa, Y., Nutzel, T., Olsen, A., Omar, A.M., Pan, N., Pandey, S., Pierrot, D., Qin, Z., Regnier, P., Rehder, G., Resplandy, L., Roobaert, A., Rosan, T.M., Rödenbeck, C., Schwinger, J., Skjelvan, I., Smallman, T.L., Spada, V., Sreeush, M.G., Sun, Q., Sutton, A.J., Sweeney, C., Swingedouw, D., Séférian, R., Takao, S., Tatebe, H., Tian, H., Tian, X., Tilbrook, B., Tsujino, H., Tubiello, F., Van Ooijen, E., Van Der Werf, G.R., Van De Velde, S.J., Walker, A.P., Wanninkhof, R., Yang, X., Yuan, W., Yue, X., Zeng, J., 2026. Global Carbon Budget 2025. Earth Syst. Sci. Data 18, 3211–3288. https://doi.org/10.5194/essd-18-3211-2026

Gattuso, J.-P., Hansson, L., 2011. Ocean acidification. Oxford university press, Oxford (GB).

Gruber, N., Boyd, P.W., Frölicher, T.L., Vogt, M., 2021. Biogeochemical extremes and compound events in the ocean. Nature 600, 395–407. https://doi.org/10.1038/s41586-021-03981-7

Gruber, N., Clement, D., Carter, B.R., Feely, R.A., Van Heuven, S., Hoppema, M., Ishii, M., Key, R.M., Kozyr, A., Lauvset, S.K., Lo Monaco, C., Mathis, J.T., Murata, A., Olsen, A., Perez, F.F., Sabine, C.L., Tanhua, T., Wanninkhof, R., 2019. The oceanic sink for anthropogenic CO2 from 1994 to 2007. Science 363, 1193–1199. https://doi.org/10.1126/science.aau5153

https://doi.org/10.5194/egusphere-2026-4577
Preprint. Discussion started: 20 August 2026

Gurvan, M., Bourdallé-Badie, R., Chanut, J., Clementi, E., Coward, A., Ethé, C., Iovino, D., Lea, D., Lévy, C., Lovato, T., Martin, N., Masson, S., Mocavero, S., Rousset, C., Storkey, D., Vancoppenolle, M., Müeller, S., Nurser, G., Bell, M., Samson, G., 2019. NEMO ocean engine. https://doi.org/10.5281/ZENODO.3878122

Guthery, S.B., 1974. Partition Regression. Journal of the American Statistical Association 69, 945–947. https://doi.org/10.1080/01621459.1974.10480233

Hirsch, R.M., Slack, J.R., Smith, R.A., 1982. Techniques of trend analysis for monthly water quality data. Water Resources Research 18, 107–121. https://doi.org/10.1029/WR018i001p00107

Ingenloff, K., Svenningsen, C., Earl, C., Shimabukuro, P.H.F., Sica, Y., Gan, Y.-M., Kachian, Z.R., Brenton, P., Hochachka, W., Wieczorek, J., Stevenson, R., Kazem, A., Baskauf, S., Zermoglio, P.F., Bloom, D., Rodrigues, A., Gamboa Martínez, J., Schigel, D., 2025. Guide for publishing biological survey data to GBIF. https://doi.org/10.35035/DOC-YNVS-EH84

Kaplanis, N.J., 2023. Insight into best practices: a review of long-term monitoring of the rocky intertidal zone of the Northeast Pacific Coast. Front. Mar. Sci. 10, 1182562. https://doi.org/10.3389/fmars.2023.1182562

Klein, E., Appeltans, W., Provoost, P., Saeedi, H., Benson, A., Bajona, L., Peralta, A.C., Bristol, R.S., 2019. OBIS Infrastructure, Lessons Learned, and Vision for the Future. Front. Mar. Sci. 6, 588. https://doi.org/10.3389/fmars.2019.00588

Knape, J., 2016. Decomposing trends in Swedish bird populations using generalized additive mixed models. Journal of Applied Ecology 53, 1852–1861. https://doi.org/10.1111/1365-2664.12720

Kroeker, K.J., Kordas, R.L., Crim, R., Hendriks, I.E., Ramajo, L., Singh, G.S., Duarte, C.M., Gattuso, J., 2013. Impacts of ocean acidification on marine organisms: quantifying sensitivities and interaction with warming. Global Change Biology 19, 1884–1896. https://doi.org/10.1111/gcb.12179

Lawrence, E., Benson, A., Biddle, M., Bosch, S., Desmet, P., Gan, Y.-M., Goldstein, P., Kennedy, M., Lillis, H., Murray, T., Perez Perez, R., Provoost, P., Sean, D., Suominen, S., Vandepitte, L., van Zweel, S., Appeltans, W., 2026. iobis/manual: v1.0 OBIS Manual bookdown version. https://doi.org/10.5281/ZENODO.20218567

Legendre, P., Gallagher, E.D., 2001. Ecologically meaningful transformations for ordination of species data. Oecologia 129, 271–280. https://doi.org/10.1007/s004420100716

Ma, D., Gregor, L., Gruber, N., 2023. Four Decades of Trends and Drivers of Global Surface Ocean Acidification. Global Biogeochemical Cycles 37, e2023GB007765. https://doi.org/10.1029/2023GB007765

Mackas, D.L., Pepin, P., Verheye, H., 2012. Interannual variability of marine zooplankton and their environments: Within- and between-region comparisons. Progress in Oceanography 97–100, 1–14. https://doi.org/10.1016/j.pocean.2011.11.002

Mackas, D.L., Thomson, R.E., Galbraith, M., 2001. Changes in the zooplankton community of the British Columbia continental margin, 1985-1999, and their covariation with oceanographic conditions. Can. J. Fish. Aquat. Sci. 58, 685–702. https://doi.org/10.1139/f01-009

Miloslavich, P., Bax, N.J., Simmons, S.E., Klein, E., Appeltans, W., Aburto-Oropeza, O., Andersen Garcia, M., Batten, S.D., Benedetti-Cecchi, L., Checkley, D.M., Chiba, S., Duffy, J.E., Dunn, D.C., Fischer, A., Gunn, J., Kudela, R., Marsac, F.,

https://doi.org/10.5194/egusphere-2026-4577
Preprint. Discussion started: 20 August 2026

Muller-Karger, F.E., Obura, D., Shin, Y., 2018. Essential ocean variables for global sustained observations of biodiversity and ecosystem changes. Global Change Biology 24, 2416–2433. https://doi.org/10.1111/gcb.14108

Muggeo, V.M.R., 2017. Interval estimation for the breakpoint in segmented regression: a smoothed score-based approach. Aus NZ J of Statistics 59, 311–322. https://doi.org/10.1111/anzs.12200

Muggeo, V.M.R., 2003. Estimating regression models with unknown break-points. Statistics in Medicine 22, 3055–3071. https://doi.org/10.1002/sim.1545

Muller-Karger, F.E., Miloslavich, P., Bax, N.J., Simmons, S., Costello, M.J., Sousa Pinto, I., Canonico, G., Turner, W., Gill, M., Montes, E., Best, B.D., Pearlman, J., Halpin, P., Dunn, D., Benson, A., Martin, C.S., Weatherdon, L.V., Appeltans, W., Provoost, P., Klein, E., Kelble, C.R., Miller, R.J., Chavez, F.P., Iken, K., Chiba, S., Obura, D., Navarro, L.M., Pereira, H.M., Allain, V., Batten, S., Benedetti-Checchi, L., Duffy, J.E., Kudela, R.M., Rebelo, L.-M., Shin, Y., Geller, G., 2018. Advancing Marine Biological Observations and Data Requirements of the Complementary Essential Ocean Variables (EOVs) and Essential Biodiversity Variables (EBVs) Frameworks. Front. Mar. Sci. 5, 211. https://doi.org/10.3389/fmars.2018.00211

O' Brien, T.D., Lorenzoni, L., Isensee, K., Valdés, L., 2017. What are Marine Ecological Time Series telling us about the ocean? A status report., IOC Technical Series. IOC-UNESCO.

Pearlman, J., Buttigieg, P.L., Bushnell, M., Delgado, C., Hermes, J., Heslop, E., Hörstmann, C., Isensee, K., Karstensen, J., Lambert, A., Lara-Lopez, A., Muller-Karger, F., Munoz Mas, C., Pearlman, F., Pissierssens, P., Przeslawski, R., Simpson, P., Van Stavel, J., Venkatesan, R., 2021. Evolving and Sustaining Ocean Best Practices to Enable Interoperability in the UN Decade of Ocean Science for Sustainable Development. Front. Mar. Sci. 8, 619685. https://doi.org/10.3389/fmars.2021.619685

Poggiale, J.-C., Baklouti, M., Queguiner, B., Kooijman, S.A.L.M., 2010. How far details are important in ecosystem modelling: the case of multi-limiting nutrients in phytoplankton–zooplankton interactions. Philosophical Transactions of the Royal Society B: Biological Sciences 365, 3495–3507. https://doi.org/10.1098/rstb.2010.0165

R Core Team, 2025. R: A Language and Environment for Statistical Computing. R Foundation for Statistical Computing.

Riebesell, U., Gattuso, J.-P., 2015. Lessons learned from ocean acidification research. Nature Clim Change 5, 12–14. https://doi.org/10.1038/nclimate2456

Rynkowski, L., Ellis, J.I., Needham, H.R., Pilditch, C.A., 2025. A systematic review and meta-analysis of the cumulative effects of multiple stressors on marine bivalves. Mar Biol 172, 96. https://doi.org/10.1007/s00227-025-04671-y

Saeedi, H., 2026. Gaps and drivers of global marine animal biodiversity from the surface to abyss. Nat Commun 17, 4553. https://doi.org/10.1038/s41467-026-73613-z

Séférian, R., Nabat, P., Michou, M., Saint-Martin, D., Voldoire, A., Colin, J., Decharme, B., Delire, C., Berthet, S., Chevallier, M., Sénési, S., Franchisteguy, L., Vial, J., Mallet, M., Joetzjer, E., Geoffroy, O., Guérémy, J., Moine, M., Msadek, R., Ribes, A., Rocher, M., Roehrig, R., Salas-y-Mélia, D., Sanchez, E., Terray, L., Valcke, S., Waldman, R., Aumont, O., Bopp, L., Deshayes, J., Éthé, C., Madec, G., 2019. Evaluation of CNRM Earth System Model, CNRM-ESM2-

https://doi.org/10.5194/egusphere-2026-4577
Preprint. Discussion started: 20 August 2026

1: Role of Earth System Processes in Present-Day and Future Climate. J Adv Model Earth Syst 11, 4182–4227. https://doi.org/10.1029/2019MS001791

Shearer, K., Hayes, J., Jowett, I., Olsen, D., 2015. Habitat suitability curves for benthic macroinvertebrates from a small New Zealand river. New Zealand Journal of Marine and Freshwater Research 49, 178–191. https://doi.org/10.1080/00288330.2014.988632

Simpson, G.L., 2018. Modelling Palaeoecological Time Series Using Generalised Additive Models. Front. Ecol. Evol. 6, 149. https://doi.org/10.3389/fevo.2018.00149

Smit, K.P., Bernard, A.T.F., Lombard, A.T., Sink, K.J., 2021. Assessing marine ecosystem condition: A review to support indicator choice and framework development. Ecological Indicators 121, 107148. https://doi.org/10.1016/j.ecolind.2020.107148

Sutton, A.J., Battisti, R., Carter, B., Evans, W., Newton, J., Alin, S., Bates, N.R., Cai, W.-J., Currie, K., Feely, R.A., Sabine, C., Tanhua, T., Tilbrook, B., Wanninkhof, R., 2022. Advancing best practices for assessing trends of ocean acidification time series. Front. Mar. Sci. 9, 1045667. https://doi.org/10.3389/fmars.2022.1045667

Sutton, A.J., Feely, R.A., Maenner-Jones, S., Musielwicz, S., Osborne, J., Dietrich, C., Monacci, N., Cross, J., Bott, R., Kozyr, A., Andersson, A.J., Bates, N.R., Cai, W.-J., Cronin, M.F., De Carlo, E.H., Hales, B., Howden, S.D., Lee, C.M., Manzello, D.P., McPhaden, M.J., Meléndez, M., Mickett, J.B., Newton, J.A., Noakes, S.E., Noh, J.H., Olafsdottir, S.R., Salisbury, J.E., Send, U., Trull, T.W., Vandemark, D.C., Weller, R.A., 2019. Autonomous seawater p CO2 and pH time series from 40 surface buoys and the emergence of anthropogenic trends. Earth Syst. Sci. Data 11, 421–439. https://doi.org/10.5194/essd-11-421-2019

Takahashi, T., Sutherland, S.C., Wanninkhof, R., Sweeney, C., Feely, R.A., Chipman, D.W., Hales, B., Friederich, G., Chavez, F., Sabine, C., Watson, A., Bakker, D.C.E., Schuster, U., Metzl, N., Yoshikawa-Inoue, H., Ishii, M., Midorikawa, T., Nojiri, Y., Körtzinger, A., Steinhoff, T., Hoppema, M., Olafsson, J., Arnarson, T.S., Tilbrook, B., Johannessen, T., Olsen, A., Bellerby, R., Wong, C.S., Delille, B., Bates, N.R., De Baar, H.J.W., 2009. Climatological mean and decadal change in surface ocean pCO2, and net sea–air CO2 flux over the global oceans. Deep Sea Research Part II: Topical Studies in Oceanography 56, 554–577. https://doi.org/10.1016/j.dsr2.2008.12.009

Tilbrook, B., Jewett, E.B., DeGrandpre, M.D., Hernandez-Ayon, J.M., Feely, R.A., Gledhill, D.K., Hansson, L., Isensee, K., Kurz, M.L., Newton, J.A., Siedlecki, S.A., Chai, F., Dupont, S., Graco, M., Calvo, E., Greeley, D., Kapsenberg, L., Lebrec, M., Pelejero, C., Schoo, K.L., Telszewski, M., 2019. An Enhanced Ocean Acidification Observing Network: From People to Technology to Data Synthesis and Information Exchange. Front. Mar. Sci. 6, 337. https://doi.org/10.3389/fmars.2019.00337

Tomal, J.H., Ciborowski, J.J.H., 2020. Ecological models for estimating breakpoints and prediction intervals. Ecology and Evolution 10, 13500–13517. https://doi.org/10.1002/ece3.6955

Toms, J.D., Lesperance, M.L., 2003. PIECEWISE REGRESSION: A TOOL FOR IDENTIFYING ECOLOGICAL THRESHOLDS. Ecology 84, 2034–2041. https://doi.org/10.1890/02-0472

https://doi.org/10.5194/egusphere-2026-4577
Preprint. Discussion started: 20 August 2026

Turk, D., Wang, H., Hu, X., Gledhill, D.K., Wang, Z.A., Jiang, L., Cai, W.-J., 2019. Time of Emergence of Surface Ocean Carbon Dioxide Trends in the North American Coastal Margins in Support of Ocean Acidification Observing System Design. Front. Mar. Sci. 6, 91. https://doi.org/10.3389/fmars.2019.00091

UNESCO/IOC, 2019. Indicator Methodology for SDG 14.3.1: Indicator description; Metadata template; Data template; Metadata instructions.[4 files]. International Oceanographic Commission of UNESCO. https://doi.org/10.25607/OBP-655

Vadas, R.L., Orth, D.J., 2001. Formulation of Habitat Suitability Models for Stream Fish Guilds: Do the Standard Methods Work? Transactions of the American Fisheries Society 130, 217–235. https://doi.org/10.1577/1548-8659(2001)130%3C0217:FOHSMF%3E2.0.CO;2

Vargas, C.A., Cuevas, L.A., Broitman, B.R., San Martin, V.A., Lagos, N.A., Gaitán-Espitia, J.D., Dupont, S., 2022. Upper environmental pCO2 drives sensitivity to ocean acidification in marine invertebrates. Nat. Clim. Chang. 12, 200–207. https://doi.org/10.1038/s41558-021-01269-2

Vargas, C.A., Lagos, N.A., Lardies, M.A., Duarte, C., Manríquez, P.H., Aguilera, V.M., Broitman, B., Widdicombe, S., Dupont, S., 2017. Species-specific responses to ocean acidification should account for local adaptation and adaptive plasticity. Nat Ecol Evol 1, 0084. https://doi.org/10.1038/s41559-017-0084

Weatherhead, E.C., Reinsel, G.C., Tiao, G.C., Meng, X., Choi, D., Cheang, W., Keller, T., DeLuisi, J., Wuebbles, D.J., Kerr, J.B., Miller, A.J., Oltmans, S.J., Frederick, J.E., 1998. Factors affecting the detection of trends: Statistical considerations and applications to environmental data. J. Geophys. Res. 103, 17149–17161. https://doi.org/10.1029/98JD00995

Wickham, H., 2016. Data Analysis, in: Ggplot2, Use R! Springer International Publishing, Cham, pp. 189–201. https://doi.org/10.1007/978-3-319-24277-4_9

Wickham, H., 2014. Tidy Data. J. Stat. Soft. 59. https://doi.org/10.18637/jss.v059.i10

Widdicombe, S., Isensee, K., Artioli, Y., Gaitán-Espitia, J.D., Hauri, C., Newton, J.A., Wells, M., Dupont, S., 2023. Unifying biological field observations to detect and compare ocean acidification impacts across marine species and ecosystems: what to monitor and why. Ocean Sci. 19, 101–119. https://doi.org/10.5194/os-19-101-2023

Wittmann, A.C., Pörtner, H.-O., 2013. Sensitivities of extant animal taxa to ocean acidification. Nature Clim Change 3, 995–1001. https://doi.org/10.1038/nclimate1982

Yang, Y., Brockmann, P., Galdino, C., Schindler, U., Gazeau, F., 2024. An update of data compilation on the biological response to ocean acidification and overview of the OA-ICC data portal. Earth Syst. Sci. Data 16, 3771–3780. https://doi.org/10.5194/essd-16-3771-2024

Yang, Y., Hansson, L., Gattuso, J.-P., 2016. Data compilation on the biological response to ocean acidification: an update. Earth Syst. Sci. Data 8, 79–87. https://doi.org/10.5194/essd-8-79-2016

Yebra, L., Puerto, M., Valcárcel-Pérez, N., Putzeys, S., Gómez-Jakobsen, F., García-Gómez, C., Mercado, J.M., 2022. Spatio-temporal variability of the zooplankton community in the SW Mediterranean 1992–2020: Linkages with environmental drivers. Progress in Oceanography 203, 102782. https://doi.org/10.1016/j.pocean.2022.102782